國立交通大學

材料科學與工程學系

碩士論文

利用邊緣移動技術研究共晶銲錫之電遷移

Electromigration study in eutectic SnPb solder by edge displacement technique

研究生：周重光

指導教授：陳智 博士

中華民國九十三年六月

利用邊緣移動技術研究共晶銲錫之電遷移

Electromigration study in eutectic SnPb solder by edge displacement technique

研 究 生：周重光　　Student：Chung-Kuang Chou

指導教授：陳　智　　Advisor：Chih Chen

國 立 交 通 大 學

材料科學與工程學系

碩 士 論 文

A Thesis

Submitted to Department of Materials Science and Engineering

College of Engineering

National Chiao Tung University

in Partial Fulfillment of the Requirements

for the Degree of

Master

in

Materials Science and Engineering

June 2004

Hsinchu, Taiwan, Republic of China

中華民國九十三年六月

利用邊緣移動技術研究共晶銲錫之電遷移

研究生：周重光　　指導教授：陳智博士

國立交通大學

材料科學與工程系所

摘要

本論文報導利用邊緣移動技術來計算共晶錫鉛受電致遷移之參數。試片結構使用經圖案化後銅/鈦結構，經由迴流與拋光銲錫形成 Blech 結構。利用原子力顯微鏡來對通電前後體積變化做計算，可獲得平均原子飄移速度。經過通電後我們觀察到在陽極部份產生突出物，陰極部份則產生孔洞。在 80 度、100 度與 120 度下施予不同電流密度，得到在 80 度、100 度與 120 度的臨界電流密度分別為-1.2×10^3 A/cm^2、-1.8×10^3 A/cm^2 及 2.9×10^3 A/cm^2,並求得活化能為 0.34eV;D_0Z^*為-9.71×10^6 cm^2/sec。

Electromigration study in eutectic SnPb solder by edge displacement technique

Student: Chung-Kuang Chou **Advisor: Dr. Chih Chen**

Department of Materials Science and Engineering
National Chiao Tung University

Abstract

In this study, we have successfully developed a technique that can precisely measure the important parameters of solder electromigration. By applying currents in the Blech specimen and by measuring the depletion volume at appropriate conditions, electromigration flux and other electromigration parameters can be obtained. We have developed a technique to fabricate solder Blech specimens, in which the depletion volume caused by electromigration can be measured precisely.

Solder Blech specimens were fabricated on patterned Cu/Ti films in Si trenches. Electromigration eutectic PbSn Blech structure has been investigated. Depletion occurred at the cathode end of the Blech sample, and hillocks were observed at the anode end for most stressing conditions. By employing atomic force microscope to measure the depletion volume on the cathode end, the electromigration rate can be measured. Drift velocity was measured at the current density ranging from 9.1 x 10^3 to 9.7 x 10^4 A/cm^2 at 80, 100, and 120 °C. The drift velocity increased when the applied current increased. The calculated threshold current density is -1.2×10^3 A/cm^2 at 80 °C, -1.8×10^3 A/cm^2 at 100 °C, and 2.9×10^3 A/cm^2 at 120 °C, respectively. The measured activation energy was 0.34 eV. With the activation energy, the values of D_0Z^* was calculated to be -9.71×10^6 cm^2/sec.

誌謝

在此要感謝所有伴我走過寶貴的兩年碩士生涯的老師同學們，首先要特別感謝我的指導教授陳智老師對學生辛勤的指導，並在我遇到困難時給予最大的支持與鼓勵。感謝謝宗雍老師、陳信文老師及高振正宏老師抽空參與我的論文口試並給予寶貴的指導。

感謝許穎超、劉書宏、楊慶榮、林鈺庭、邱聖翔和劭棟樑學長，給予實驗製程上的指導及幫忙，感謝陳德聖和黃淵明同學，一起努力為畢業打拼，幫我照SEM，另外，感謝學弟黃章斌、尤宏誌及學妹陳筱芸，專題生梁世緯，熱情校友林佳輝，以及實驗室畢業的學長姐們和曾經是專題生的學弟妹們，有這一群實驗室的人們才讓我的研究生活充滿活力歡笑及點滴回憶，一路走來的吃吃喝喝與玩樂是最好的記憶。同時感謝林宏洲老師和吳耀銓老師的學生們，一起打球的歡樂。還有我大學時代的朋友們，有他們在生活上的陪伴，讓我在最累的時候還有持續的力量。一切曾幫過我的人們，謝謝你們。

最後、感謝一直支持著我的父母、弟弟與妹妹，你們的支持是我做研究的精神支柱，讓我無後顧之憂的完成我的學業，千言萬語僅以一句謝謝表示，謝謝!

Table of Contents

List of figures

List of table

Chapter 1 Introduction

1.1 An overview of solder in flip chip technology

Microelectronic packaging is about how to connect the circuitry on a Si chip to the outside world. Both wire bonding and solder bumping technologies have been used. The trend in microelectronic packaging is to a wider use of solder bumping. One of the advantages of solder bumping over wire bonding is that a larger number of tiny solder bumps can be made into an area array on a chip surface as input/output (I/O) interconnections. Today, the diameter of solder bumps is 100 μm and the pitch between them is 100 μm, so on 1 cm^2 chip surface, we can have 2500 I/O bumps. If the bump diameter and pitch are reduced to 50 μm, we can have 10,000 bump/cm^2. This aerial density meets the projected I/O requirement in the next ten years as given in International Technology Roadmap for Semiconductors by Semiconductor Industry Association. [1] Figure 1(a) shows the scanning electron microscopic image of an array of solder bumps on a Si chip.

The solder alloy of 95 wt. % Pb and 5 wt. % Sn (95Pb5Sn) has been used as solder bumps on Si chip surfaces in mainframe computers. [2] To join a chip to a ceramic module, as shown in Fig. 1(b), the chip is flipped up-side-down, i.e., the side having the active very-large-scale-integration (VLSI) of devices faces down. It is known as the flip chip technology. Then the ceramic module is joined to a printed circuit board using a second set of solder bumps, which is eutectic SnPb solder (or a composite solder) and the bump size is much bigger, as shown Fig. 1(b). Eutectic SnPb solder (38 wt. % Pb and 62 wt. % Sn) is used in the second set because it has a much lower melting point (183 °C) than that of the 95Pb5Sn solder (320 °C). Hence the high-Pb solder bumps do not melt during the

joining of the eutectic bumps. This is a two-level packaging scheme used in mainframe computers; first chip-to-ceramic and then ceramic-to-polymer. [2, 3] In this thesis, we use eutectic the tin-lead solder, which has been used and studied for many years, in chip-to-board packaging. [4, 5]

Lead plays an important role in SnPb solders. It provides ductility and a shining surface. Also, it lowers the interfacial energies of the solder. therefore the eutectic SnPb solder has a very low wetting angle of 11° on Cu, while the wetting angle of pure Sn on Cu is 35. Furthermore, the interfacial energy between the molten solder and the Cu_6Sn_5 intermetallic compound (IMC) is low. Finally, the high-Pb solder has a very narrow temperature gap.

When the low-cost and large-volume consumer electronic products are up-graded by using advanced chips for better performance, more I/O will be needed. To eliminate the high-cost ceramic module, High-Pb solder can no longer be used due to the lower glass transition temperature of organic substrates. Eutectic PbSn is used instead due to its low melting temperature, good reflow characteristic and high mechanical performance.

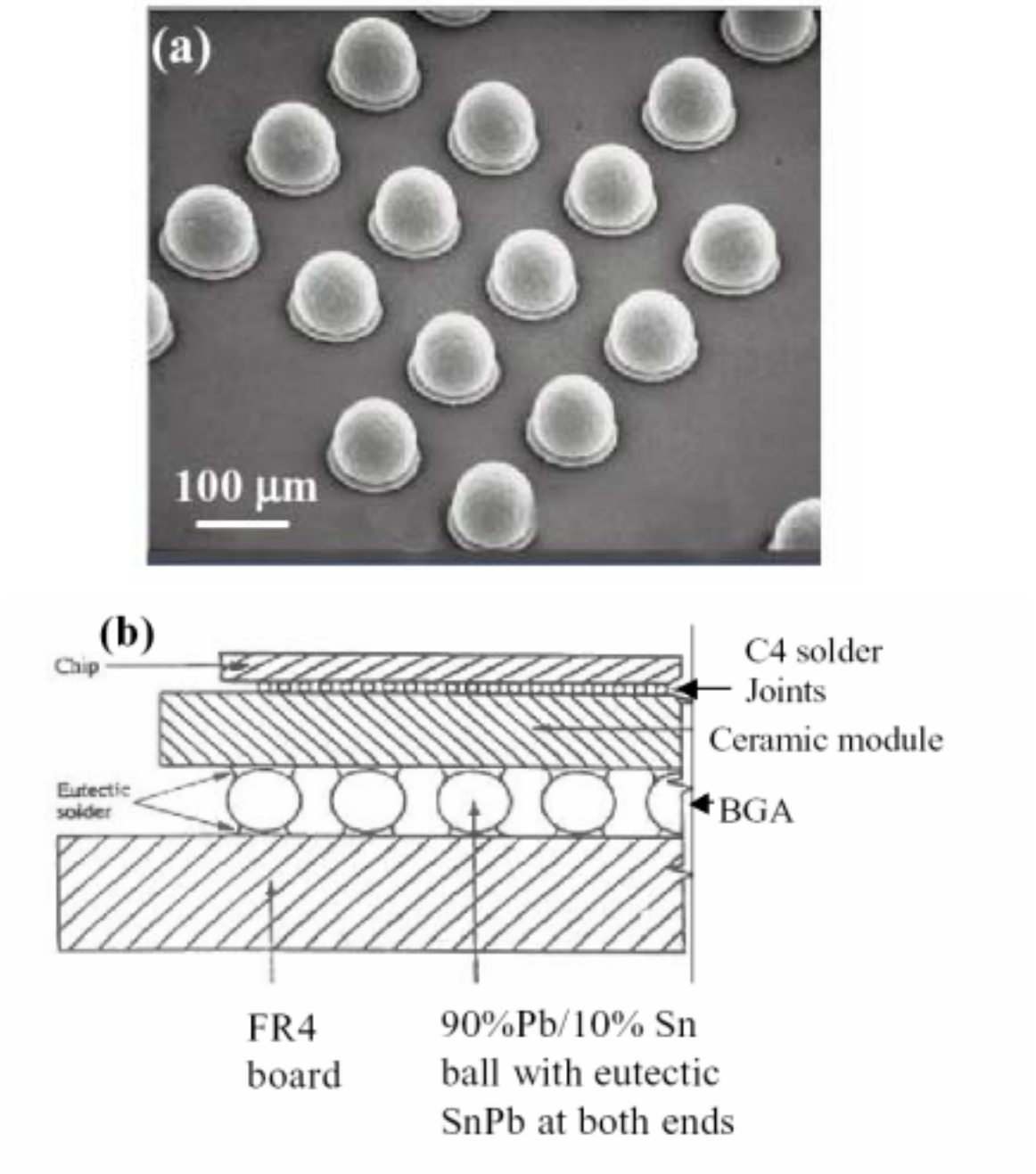

Fig. 1 (a) An area array of solder balls on a Si chip surface (Courtesy of W. J. Choi, UCLA). (b) The cross-section of a two-level packaging; chip-to-ceramic module and ceramic module-to- polymer board, where C-4 solder joints are solder joints and BGA is ball-grid-array.[2]

1.2 Eutectic SnPb Solder Reactions

Intermetallic Compound (IMC) Formation

The eutectic SnPb reacts with the metallization layer to form intermetallic compounds (IMCs) in during reflow process. When the eutectic SnPb solder reacts with Cu at 220°C, the reaction products are Cu_6Sn_5 and Cu_3Sn IMCs. This is in agreement with the ternary phase diagrams of Sn-Pb-Cu shown in Fig. 2. And the morphology of Cu_6Sn_5 is hemispherical-shape and the Cu_3Sn IMC in layer-shape.

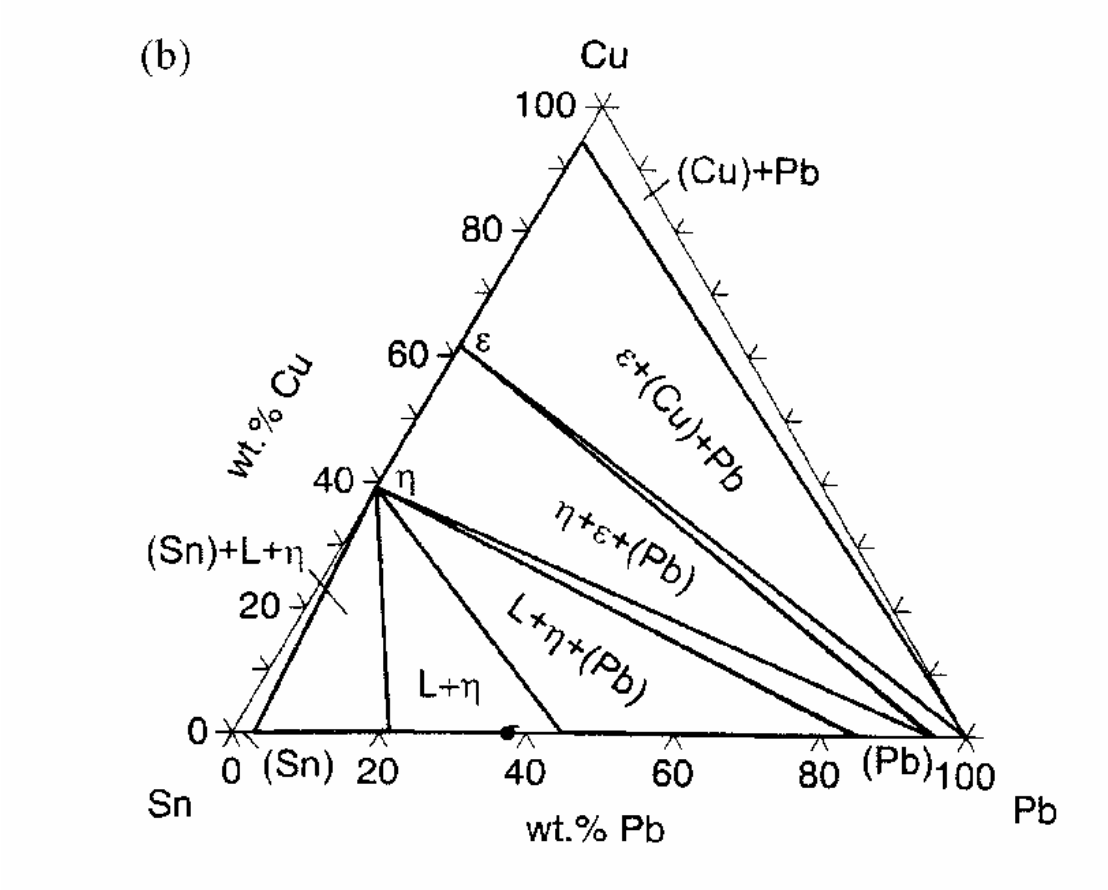

Fig 2 Ternary phase diagram of Sn-Pb-Cu at 200 °C[2]

The Cu_6Sn_5, however, is unstable on the surface of thin Cu-Ti film, leading to the spalling of Cu_6Sn_5 IMC. When Cu is consumed, shown Fig. 3. The transformation from a hemispherical-shape to a sphere-like was driven by lowering the sum of surface and interfacial energies in a conservative ripening.[3]

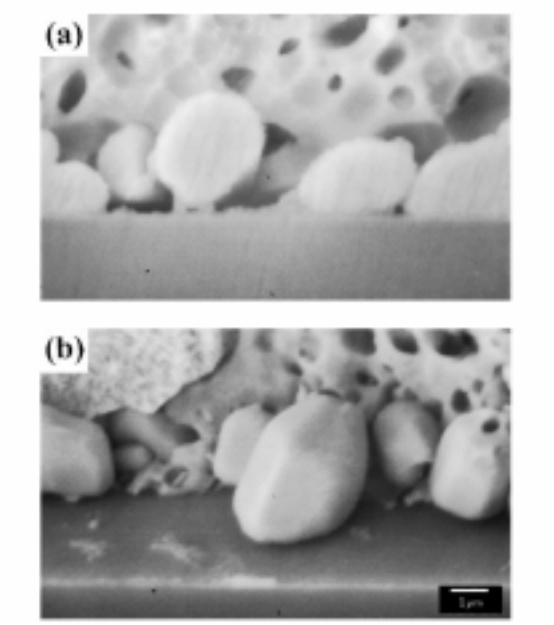

Fig.3 Cross-sectional SEM image of the formation of spheroid-typeCu_6Sn_5 at the interface between eutectic SnPb and 870nm Cu/100nm Ti thin film under-bump-metallization (UBM) after 10min at 200°C(a)2D image;(b)3D image after etching away the solder [3].

1.3 Electromigration theory

Electromigration is the atomic motion in a metal under the influence of an applied electric field. It is basically a diffusion phenomenon under a driving force. This atomic motion is driven by the sum of two diametrical force acting on a metal atom: One is the direct force due to the Coulomb interaction of the positive metal ions with the electric field in the conductor. And another is so-called electron wind force which results from the momentum transfer between the electrons and the metal ions. Depending on which of the force is stronger, the atoms move towards the cathode or anode end of the conductor. In general, the electron wind force is stronger than the direct force for a good conductor and the atoms move to the anode end of the conductor.

Atomic diffusion flux in solid can be represented by

$$J = -D\frac{\partial C}{\partial x} + \sum_i CM_i F_i \quad \text{.....(1.1)}$$

Where the first term comes from the chemical potential gradient and the second term is the sum of various applied forces. For electromigration in a pure metal, the chemical gradient term is removed. And the resulting force F_{EM} due to electromigration is conventionally expressed as the product of the electric field E and the effective charge Z^*e[4].

$$F = EZ^*e \quad \text{.....(1.2)}$$

Where Z* is the effective valence number of the metal atom [5] and e the fundamental charge.

The atomic flux J_{EM} due to the electromigration driving force F_{EM} can be written as [1],

$$J_{EM} = CMF_{EM} \quad \text{.....(1.3)}$$

where m is the mobility of the atoms and C the atomic concentration. The mobility M of the atoms is given by the Einstein equation

$$M = \frac{D}{kT} \quad \cdots\cdots (1.4)$$

where D is the diffusivity, k Boltzmann ' s constant and T the absolute temperature. Therefore, the atomic flux due to electromigration can be expressed as

$$J_{EM} = C\frac{D}{kT}Z^{*}eE = C\frac{D}{kT}Z^{*}e\rho j = C(\frac{D_0}{kT})\exp(\frac{-E_a}{kT})Z^{*}e\rho j \quad \cdots..(1.5)$$

where j is the current density, ρ the diffusivity of the metal and E_a activation energy.

1.4 Measurement of electromigration

Diffusion measurement

The first type of measurement is similar to the usual diffusion measurement except that the sample has to be shaped to allow the flow of current with a sufficient current density to produce a measurable amount of electromigration. The principle of this type of measurement is shown in Fig. 4.

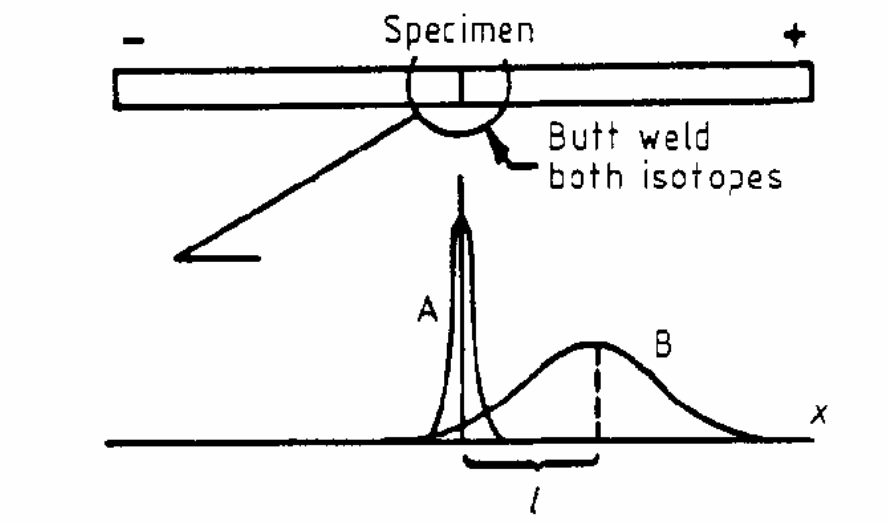

Fig. 4. The isothermal isotope method: **A,** inert marker concentrations; **B,** concentration of matrix isotope. (From Huntington **(1974)).**

For bulk studies, the sample is usually made into a cylindrical form with liquid cooling of both ends. The element to be measured can be incorporated uniformly into the sample or inserted near the center of the sample. Upon passage of the current, the composition distribution will change as a result of electromigration. [6] The concentration profiles of the tracer before and after electromigration are depicted in Fig. 4 by the curves A and B, respectively. The distance between the centroid of A and B divided by the annealing time gives the drift velocity, from which the DZ* can be determined. The spreading of curve B with respect to A determines D; the tracer diffusion is a random walk. The difficulty of carrying out such an experiment is to maintain a uniform temperature over the entire sample, for otherwise a correction due to the effect of temperature gradient is required. [7]

The second type of measurement is called the 'vacancy flux' method which measures the change in the sample dimension as a result of the creation and annihilation of vacancies along the sample during the course of electromigration. The principle of this measurement is illustrated in Fig. 5. The early experiments simply measured the displacement of surface markers (scratches or indentations) separated by a uniform spacing along the length of a wire sample (Huntington and Grone 1961). Later, in a study of A1 (Penney 1964), it became apparent that the change in the dimension is not confined to being along the length of the sample only; there are also transverse dimensional changes. The latter was found to depend on the aspect ratio of the sample and should be included to account for the total vacancy flux. The simplicity of the measurement has made this method one of the principal techniques in electromigration studies and it has been applied to measure bulk electromigration for a large number of pure elements. Results of these measurements are in general agreement, although not with the same accuracy, as those obtained from chemical analysis.[6]

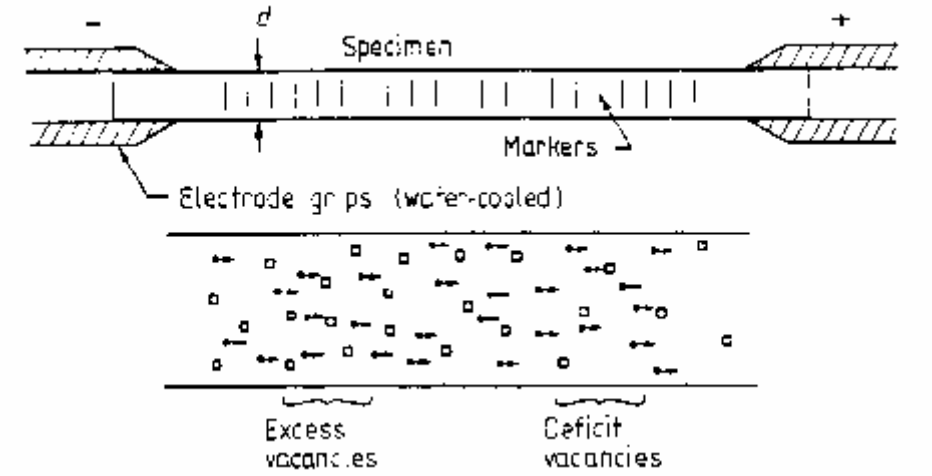

Fig. 5 Vacancy flux method-schematic experiment: · electron, □ vacancy. (From Huntington (1974))

Edge displacement technique (Drift velocity method)

The mass transport of electromigration in a thin metal film can be investigated directly using the drift velocity method [8-10]. The experiment is also called the " saddle movement experiment. " It was first presented by Blech in 1975 and as been widely adopted since then for the study of atomic drift velocity, the direction of the mass transport, and the activation energy, as well as other parameters.

A sample configuration for the drift velocity experiments is shown in Fig. 6. Basically, a piece of metal track. For example, the metal film studied in the first drift velocity experiment [8] was Au while the metal track was Mo. A constant current is applied through the metal track, and most of the current is diverted into the highly conducting Au saddle in the overlapped region. As a result, the saddle experiences a continuous impulse from the electron wind force, in the direct from the cathode to the anode edge.

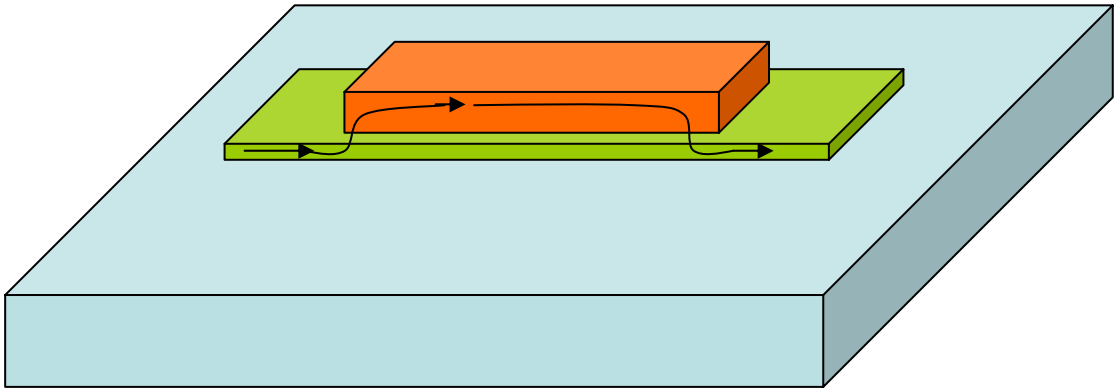

Fig. 6 Schematic of sample configuration for drift velocity measurements.

The mass in the saddle will therefore be transported in that direction, which is obtained from the effective movement of the saddle edge along the metal track. This average atomic drift velocity is given by

$$v = \frac{J}{C} = (\frac{D_0}{kT}) \exp(\frac{-E_a}{kT}) Z^* e \rho j \quad \text{.....(1.6)}$$

where v is the drift velocity, J is the atomic flux, and ρ is the Resistivity of the film. Equation (1.6) also can be rewritten as

$$\ln(\frac{vt}{j}) = \ln(\frac{D_0}{kT} Z^* e \rho j)(\frac{-E_a}{kT}) \quad \text{.....(1.7)}$$

Thus, measurement of drift velocity at various temperatures yields the value of activation energy. Equation (1.6) also indicates that measurement of the D_0Z^* product is possible if the drift velocity is measured as a function of the current density [11].

A threshold current density exists for electromigration is found by I.A. Blech and is shown in Fig. 7 [9]. This current is approximately inversely proportional to stripe length. The occurrence of the threshold is explained by opposing chemical gradients created by the atom pile-up and depletion at the stripe ends. The threshold is increased by decreasing the temperature or by enclosing the aluminum in silicon nitride. K. N. Tu *et al* proposed that in current crowding, the current-density gradient can exert a driving force strong enough to cause excess vacancies point defects to migrate from high to low current-density regions. This leads to void formation in the latter [12].

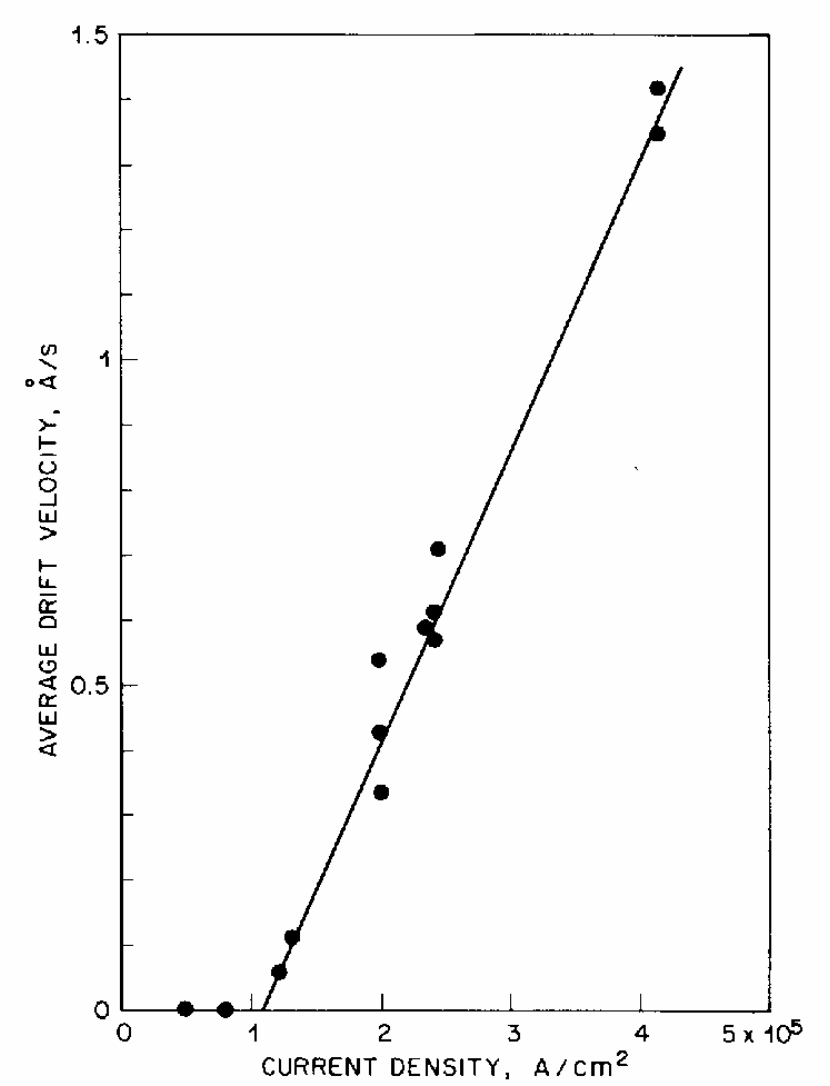

Fig. 7 Average drift velocity of an aluminum stripe as a function of current density [7].

Resistometric measurement

The resistance of a metal interconnect in integrated circuits is sensitive both to its microstructural and geometrical parameters. When electromigration creates voids, cracks, or hillocks within a metal line, the line microstructure and geometry are distorted and the line resistance changes. This techniques is suitable for study of the early stage of electromigration, where the conditions of uniform current density and temperature have not been disturbed significantly. Under the assumption of the early stage of electromigration, that is, the dimensions of the maximum voids are much less than the line width-it is

straightforward to show that the line resistance of a thin film conductor has the following form [12]:

$$\frac{\Delta R}{R} = \frac{R - R_0}{R_0} = Cj^n \exp(\frac{-Ea}{kT}) \cdots\cdots(1.8)$$

Where R_0 is the line resistance at a reference temperature, C is a constant depending on the film geometry, the grain boundary structure, and the grain size, t is the time that the conductor has been stressed, Ea is activation energy, k is Boltzmann's constant, and T the absolute temperature. As indicated by Eq. 1.8, at a fixed current density j resistance measurements at different temperatures provide information on the value of the activation energy Ea, and the measurements at different current density levels determine the value of the exponent n. [6]

J.Y. Choi, S.S. Lee and Y.C. Joo reported that electromigration characteristics of eutectic SnPb solder which using thin stripe-type test structures in which the temperature and the current density were varied from 80 to 100°C and from 4.6 to 8.7 10^4 A/cm^2. They assumed that the electromigration-induced drift of the solder materials is the main cause of the initial resistance change; it can be assumed that the normalized rate of change in resistance is proportional to the electromigration-induced flux shown in eq. (1.7). Rewritten the equation, as

$$\ln(T \cdot Normalized\_rate) = -\frac{E_a}{kT} + const \cdots\cdots..(1.9)$$

The activation energy of electromigration can be obtained by plotting ln(T. nomalized rate) vs 1/T, as seen in Fig. 8. The calculated activation energy is 0.77 eV.[13]

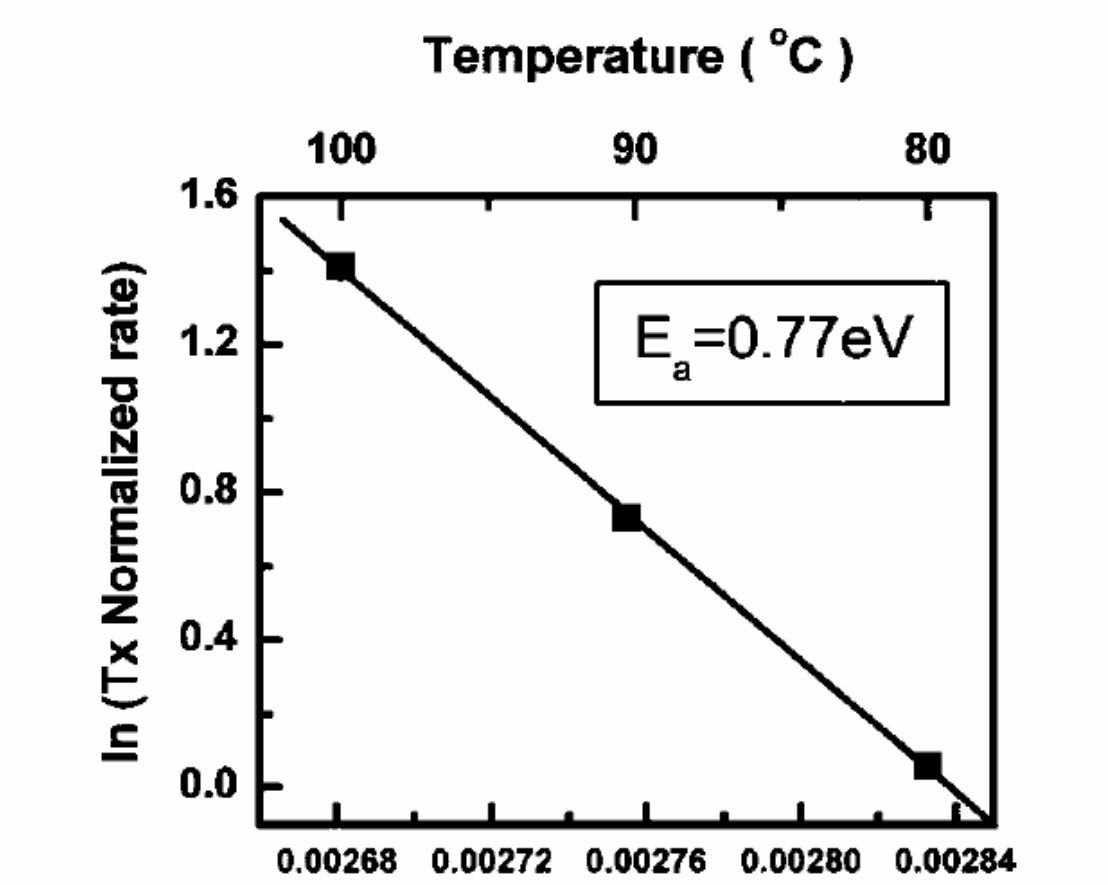

Fig. 8 Calculation of activation energy for electromigration of eutectic SnPb solder from initial rate for change[13]

Mean Time to Failure

In 1969, Black provided the following equation to analyze failure in Al interconnects caused by electromigration.[14]

$$MTTF = A\frac{1}{j^n}\exp(\frac{Ea}{kT}) \cdots\cdots(1.10)$$

The derivation of equation was based on an estimate of the rate of forming voids across an Al interconnect. The most interesting feature of the equation is the dependence of MTTF on square power of current density, i.e., n=2. In essence, Black assumed that the rate of mass transport in electromigration is proportional to electron momentum and number of electrons per unit area per unit time. Both of them are proportional linearly to current density, hence the square power dependence. In MTTF equation, whether the exponent n is 1, 2 or a large number has been controversial, especially when the effect of

joule heating is taken into account. However, assuming that mass flux divergence is required for failure, the nucleation and growth of a void requires vacancy super-saturation, Shatzkes and Lloyd have proposed a model by solving the time-dependence diffusion equation and obtained a solution for MTTF in which the square power dependence on current density is also obtained.[15] However, whether Black ' s equation can be applied to MTTF in Cu interconnects and flip chip solder joints deserves a careful examination.

Electromigration of eutectic SnPb flip chip solder joints and their mean-time-to-failure have been studied in the temperature range of 100 to 140 °C with current densities of 1.9 to 2.75 $\times 10^4$ A/cm^2 by W. J. Choi, E. C. C. Yeh, and K. N. Tu. In these joints, the under-bump-metallization (UBM) on the chip side is a multilayer thin film of Al/Ni(V)/Cu, and the metallic bond-pad on the substrate side is a very thick, electroless Ni layer covered with 30 nm of Au. When stressed at the higher current densities, the MTTF was found to decrease much faster than what is expected from the published Black ' s equation. When the measured MTTF is plotted against temperature ($T+\Delta T$) which Joule heating was considered as shown in Figs. 9(a) and 9(b), the calculated activation energy Q is found to be 0.5 and 0.8 eV for the eutectic SnPb solder and eutectic SnAgCu solder, respectively.[16]

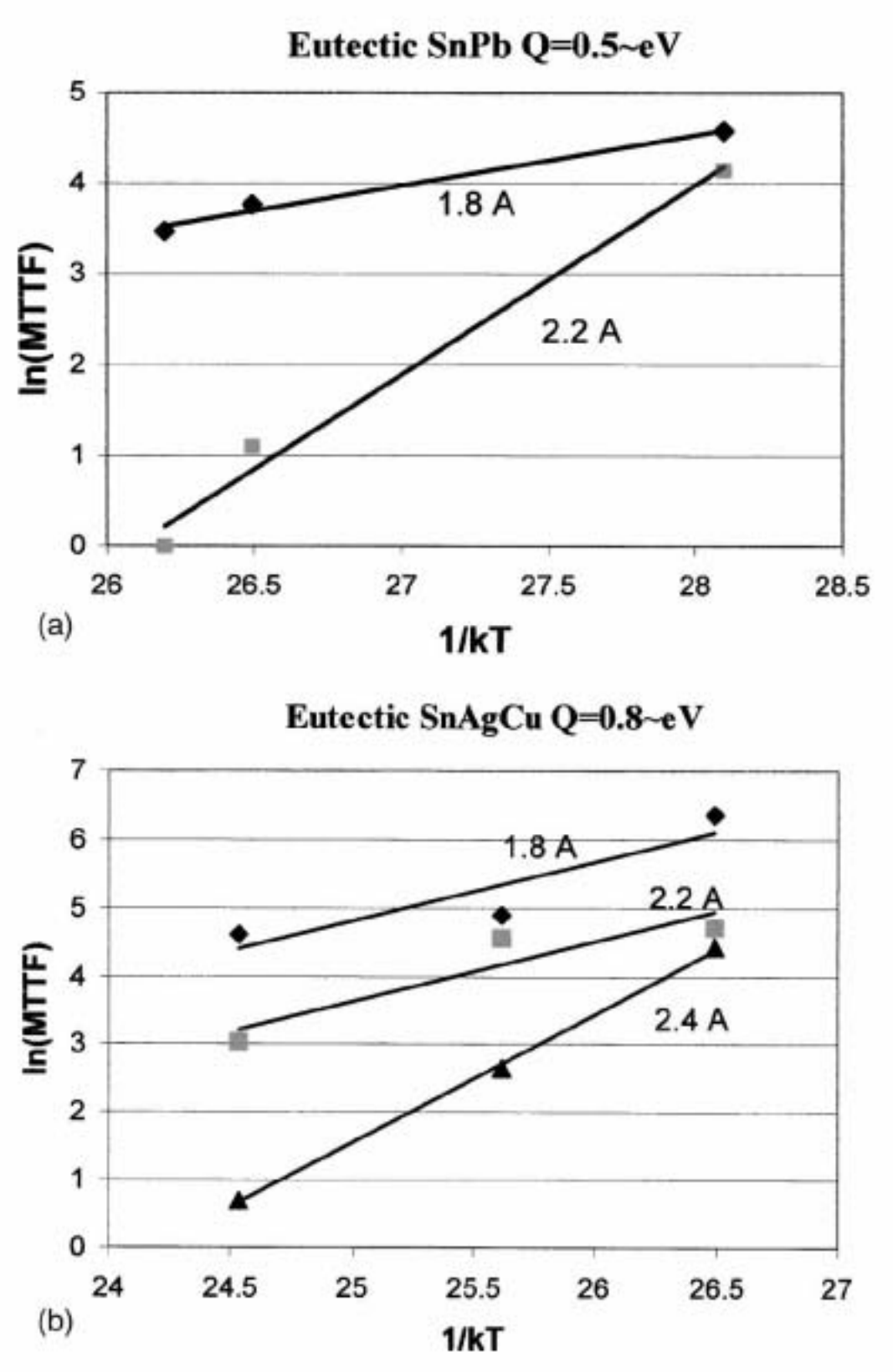

Fig. 9. Plots of MTTF against $1/k(T+\Delta T)$, where ΔT is the temperature increase due to Joule heating: (a) eutectic Sn Pb solder joints, and (b) eutectic SnAgCu solder joints.[16]

1.5 Motivation

In general, electromigration in solder can be expressed as the following equation [7]:

$$J_{EM} = CDZ^{*}eE = C(\frac{D_0}{kT})\exp(-\frac{E_a}{kT})Z^{*}e\rho j$$

where J_{EM} is the electromigration flux, C is the concentration of atoms per unit volume of the eutectic alloy, D is the effective lattice diffusivity of the solder at testing temperature, Z^* is the effective charge number, E is the electric field, D_0 is the prefactor for the diffusivity, E_a is the activation energy for electromigration, ρ is resistivity of the film, j is the current density, k is the Boltzmann's constant, and T is the absolute temperature. Blech developed a technique for measurement of the electromigration parameters. The specimen used was a patterned conductive film coated on a patterned resistive film [9], which is denoted as the Blech specimen in this letter. By applying currents in the Blech specimen and by measuring the depletion volume at appropriate conditions, electromigration flux and other electromigration parameters can be obtained. In particular, by measuring the electromigration flux at various current densities, threshold current density can be obtained by extrapolating to the zero drift velocity. The threshold current density for solder electromigration is a very important parameter, since it represents the maximum current density that a solder joint can carry without the occurrence of electromigration.

There have been many studies on the electromigration of solder joints [17-22]. Damage due to electromigration occurs when the solder joints are stressed by the current density of 5×10^3 A/cm^2 and above. Electromigration rate of Pb-containing solders was measured by applying currents in thin strips for solder lines [18]. Effective charge number of eutectic solder was measured to be 33 for V-groove solder lines stressed by estimating the hillock volume generated under a current density of 2.8×10^3 A/cm^2 at 150

°C [19].

However, most of the important electromigration parameters of solders are still unknown due to the difficulty in measuring precisely the electromigration rate. Since most of the previous studies used film, line or bump specimen for electromigration investigation, the volume of hillocks or voids was estimated by a scanning electron microscope (SEM). In addition, because most of the solders cannot be fabricated by conventional deposition methods, Blech specimens can not be easily prepared. Nevertheless, we have developed a technique to fabricate solder Blech specimens, in which the depletion volume caused by electromigration can be measured precisely. Thus, it expedites the scientific study of electromigration in solder.

Chapter 2 Experimental

2.1 Fabrication of Blech Structure

a. Substrate preparation: The substrate used in this experiment is n-type four-inch (100) wafer.

b. Photolithography I: 1st – level mask was applied to define the indentation of strips. AZ5214 photoresist was spin-coated on the sample. Then the sample was soft-baked at 100°C for 1 minutes, followed by exposure. The photoresist which was exposed was removed by FDH 5 developer, afterwards the sample was hard baked for 7 minutes at 120°C.

d. Silicon dry etching: The inductively coupled plasma-reactive ion etching (ICP-RIE) technique was used to dry etching silicon. The depth of etching that was measured by α -stepper and Atomic Force Microscopy (AFM) was 3.1 μm.

e. Deposition SiO_2 and metal: To prevent leak current, an insulator layer of SiO_2 on the silicon wafer was grew oxides of 1200A by wet oxidation method. Then 1500A Ti and 4000A Cu was deposited by E-gun evaporator.

e. Photolithography II: 2nd-level mask was applied to define the Cu lines, which were used for wetting solder.

f. Copper etching: Copper film was stripped away by the solution $FeCl_3$+D.I. Water (1:200).

g. Reflow solder: Eutectic PbSn was reflowed at 210°C for 4 sec on the hot plate. Solder wetted only on Cu and formed Cu_6Sn_5 which was confirmed by energy dispersive spectroscopy (EDX).

h. Polish solder: Samples were polished to achieve Blech-like structure. The corresponding schematics are show in Fig. 10(a) through 10(h). Tilted plan view of the structure is shown in Fig. 11

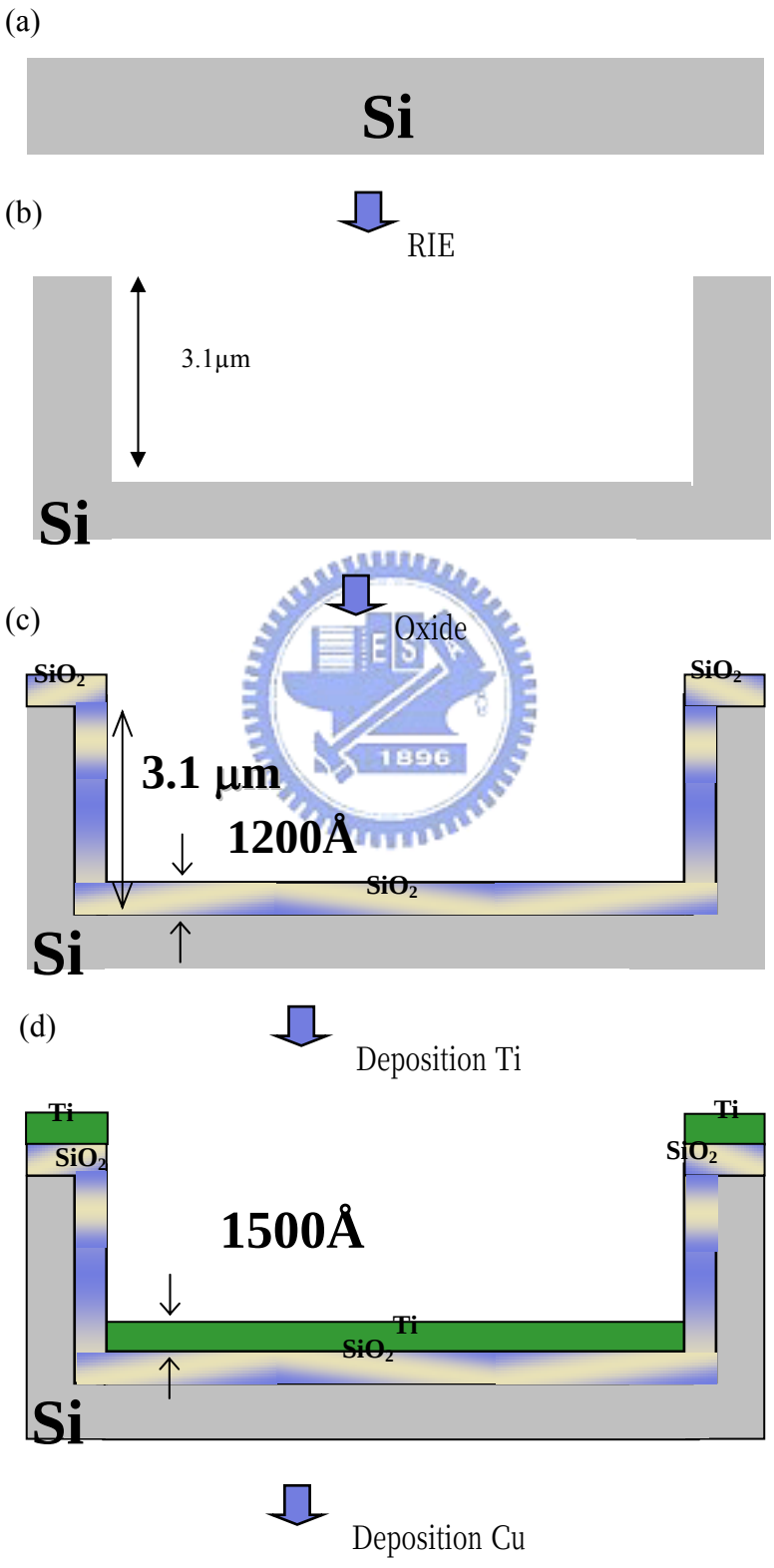

(e)

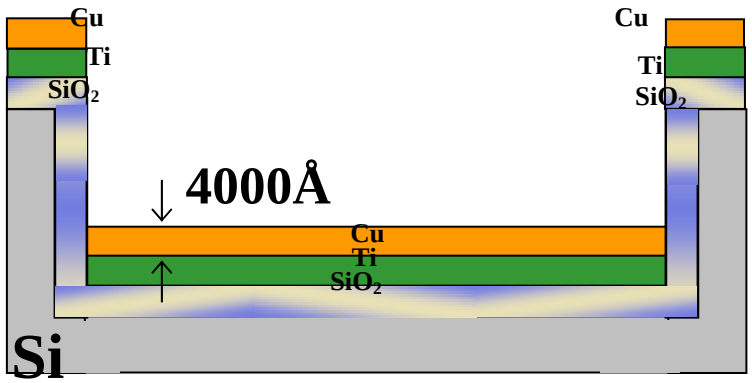

(f)

Patten Cu

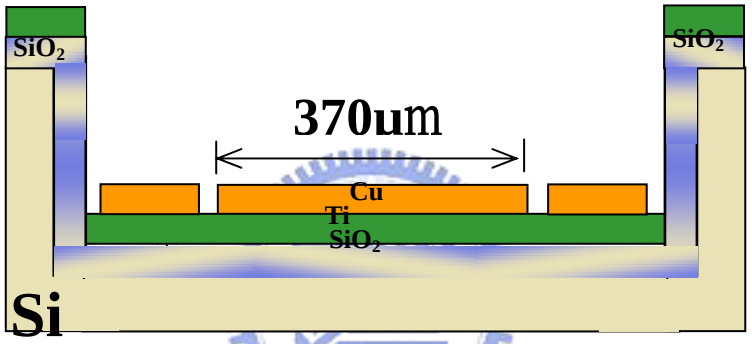

Reflow solder

(g)

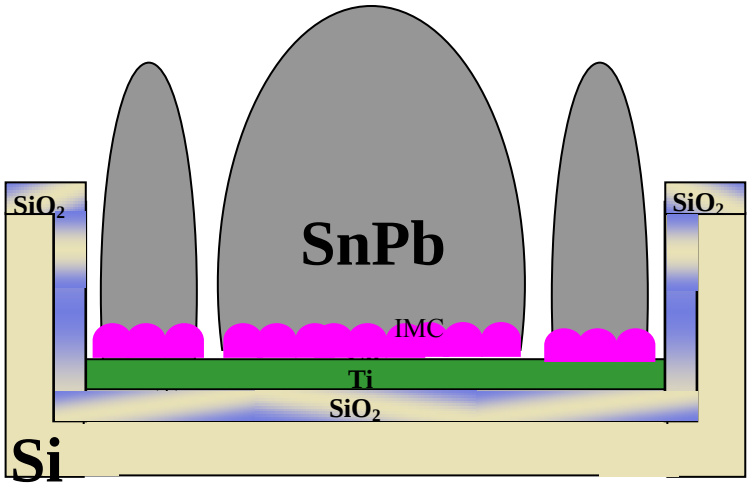

Polish

(h)

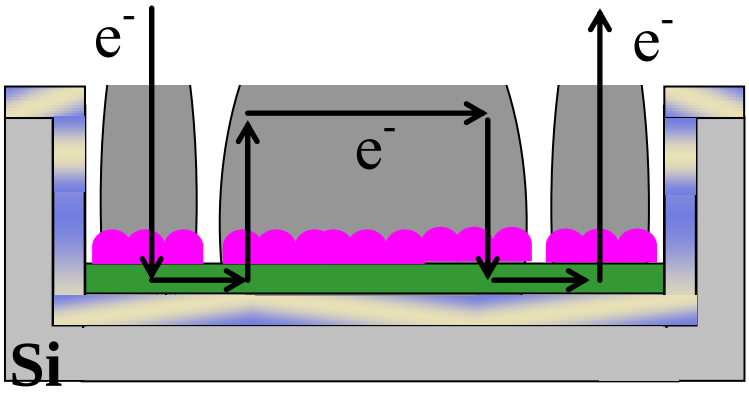

Fig. 10 Schematic drawing of Fabrication of Blech Structure

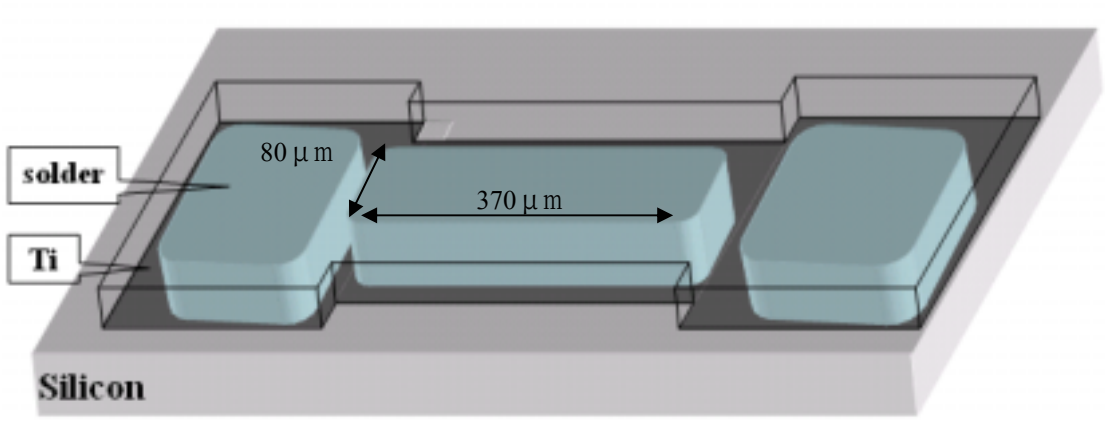

Fig. 11 Schematic drawing of tilted plan view of the test sample

2.2 Conditions of current stressing

The effective current density in the SnPb layer was calculated for each sample using a parallel circuit model (Fig. 12) on the basis of resistivity thickness of the Ti, IMC and the SnPb layers. Their resistivities are shown in Table 1.The IMC thickness can be measured by scanning electron micro scope (SEM) or transmission electron microscope (TEM) cross section images. Before current stressing, the surface profile near the cathode was measures by atomic force microscope. Thus, the thickness of the SnPb solder can be obtained by subtracting the thickness of the structure from the thickness of the IMCs. Varied stressing conditions were investigated in this study, as shown in Table 2. Figure 11 shows the schematic drawing of a test sample. Figure 13 shows the experimental setup, which depicts the sample in a probe station connecting to a current source. Current was applied by the two probes. The current source used in this study is Keithley 2400 I-V source meter. The resolution of the current output is 500nA.

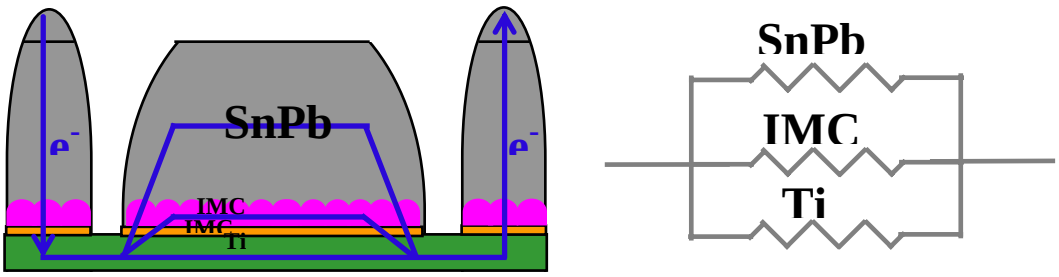

Fig. 12 Effective parallel circuit model for the SnPb Blech samples.

Material	Resistivity(μΩ-cm)
Eutectic SnPb	14.5
Ti	42
Cu_6Sn_5	17.5

Table 1 Resistivity used in calculating Current density

Current density (A/cm^2) / Temperature°C	$1*10^4$	$3*10^4$	$5*10^4$	$6*10^4$	$8*10^4$
80°C	162hrs		72hrs		72hrs
100°C	144hrs	72hrs		72hrs	
120°C	72hrs	72hrs			

Table 2 List of testing conditions of current stressing

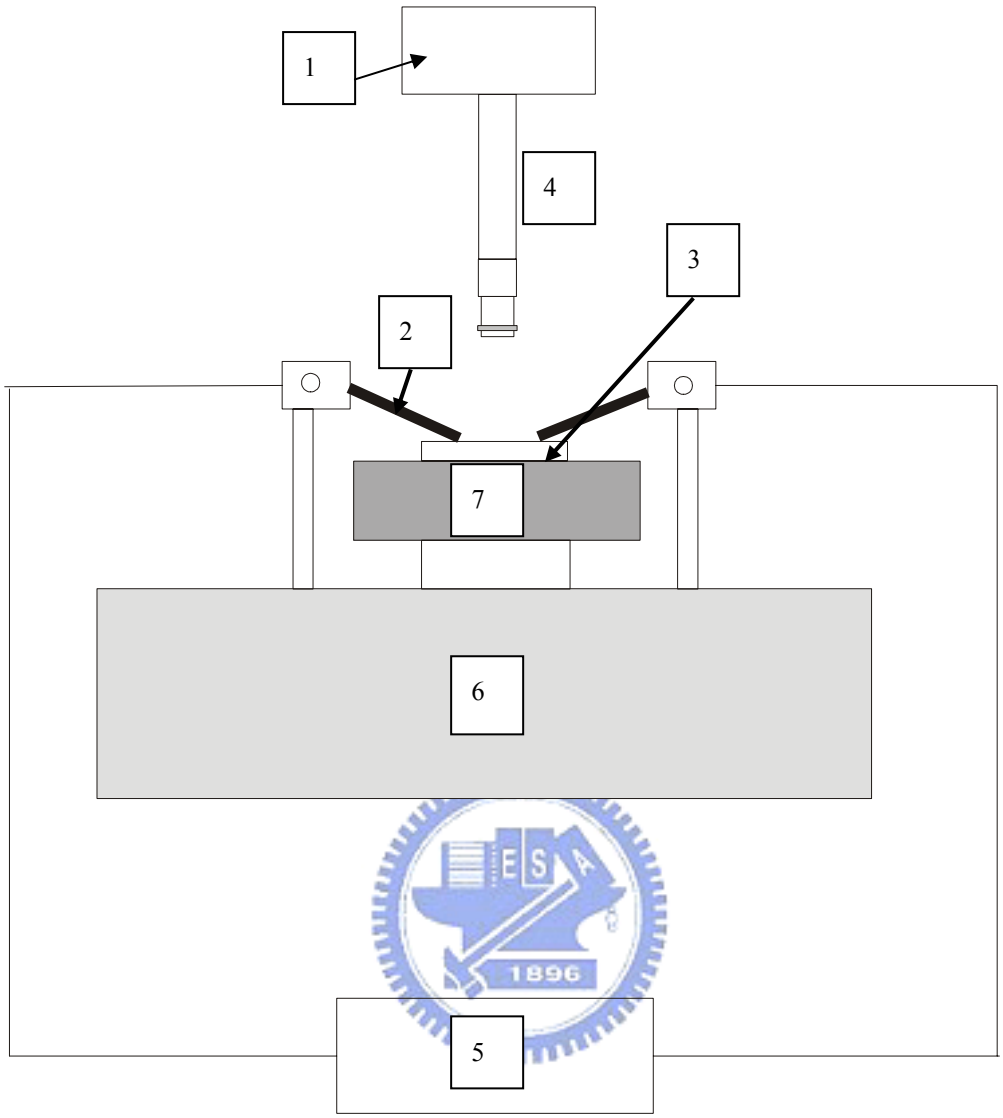

1. CCD camera 2. Probe 3. Sample 4. Optical lens 5. Current source
6. Stage 7. hot plate

Fig. 13 Schematic drawing of the sample in a probe station connecting to a current source.

2.3 Analysis Techniques

a. **Scanning Electron Microscopy (SEM):** SEM is one of the useful surface analytical techniques. By using SEM, hillock as well as the evolution of the microstructure before and after the stressing by the direct electrical current was characterized. We observed the morphology change in the sample using a JOEL 6500f field emission SEM.

b. **Optical Microscopy (OM):** Microstructure and rough inspection were made by OLYMPUS BH2-UMA OM.

c. **Atomic Force Microscopy(AFM):** AFM produces high resolution, three-dimensional images by scanning a sharp tip over the sample surface. The tip is part of a fexible cantilever mounted on one end of a cylindrical piezoelectric tube mounted near the top of the microscope. Voltages applied to the X and Y electrodes on the piezoelectric tube detect the tube horizontally to produce a precise raster scan over the sample surface. A voltage applied to the Z electrode on the piezo tube controls the vertical height of the tip. A stepper motor coupled to a lead screw translates a slide with the sample attached. A separate motor driven controls the height of the microscope and the tip relative to the sample surface. We use AFM (Digital Instruments Dimension 3100) to measure the depletion volume caused by current stressing.

d. **Energy Dispersive X-ray Detector (EDX):** EDX is one of the chemical analysis techniques. EDX (JOEL 6500f in National Chiao Tung University) was used to investigate composition of IMC.

e. **α-stepper (Surface profile) :** The thickness of sample was also measured by α-stepper. The α-stepper used in this study is Dektak II A in Materials Science and Engineering in NCTU.

f. **Infrared scope (InfraScope)：** The temperature increase due to joule heating effect was measured by a infrared microscope. The temperature measurement is comprised of three steps: First: it acquire an radiance reference image without current stressing, which was used to find and map the sample emissivity at each pixel. Second: It acquires an temperature image without current stressing to check the set-up. Third: It takes a temperature image with current stressing to record the device temperature. The temperature was calculated by Planck ’ s Law.

Chapter 3 Results and discussion

3.1 Joule heating during current stress

The temperature maps were measured as a function of applied current at various ambient temperatures, as shown in Figs. 14、15 and 16. With increasing current, the solders temperature slightly increased but no more than 2°C. However, when the applied current is greater than 0.1A, serious joule heating occurred at the Ti film. Therefore, the applied current were kept under 0.1 A.

Figure 14 (a) shows the sample under the current stressing of 0.01 A on a 80°C hot plate. The measured average temperature in solder stripe during the current stressing was 80.35 °C, i.e., the temperature increase due to joule heating under the current stressing 0.01A on a 80°C hot plate was 0.35 °C. Figure 14 (b) shows the sample under the current stressing 0.02 A on a 80°C hot plate. The temperature increase due to joule heating under the current stressing was 0.49°C, which is higher than that of the current stressing at 0.01A. As the applied current increasing to 0.03A, the measured temperature increase was 0.51 °C. As shown in Fig. 14 (c), the temperature of right edge in solder stripe was 76 °C and the temperature of left edge in solder stripe was 82 °C. These values were not correct because the infraccope use radiation to estimate temperature and it ’s sensitive to surface condition. It needs a flat surface to obtain reasonable data. Therefore, we took the temperature data inside the solder stripe and avoided using the data at edge or particle. When applied current reached 0.1 A, the temperature in Ti film was obvious higher than that in solder, as shown in Fig. 14 (i). Figure 17 (b) shows the temperature profile along the white line in Fig. 17(a), and the temperature in Ti film was 86°C, while 81.4 °C for solder. Figure 15 (b) shows the sample under the current stressing of 0.02 A on a 100°C hot plate. The particles in solder

which came from polish process had unreasonable temperature. It may be also owing to rough surface of the particle. With increase of applied current, the temperature increase in Ti film, as shown in Fig. 15 (j). Figure 16 (a) shows the sample under the current stressing of 0.01 A on a 120°C hot plate. The measured temperature in the solder stripe was 120.17 °C. When the sample was stressed by 0.07 A on a 120°C hot plate, the temperature increase was as high as 123.79°C. Therefore, to prevent from damaging the Ti film, the applied current was kept below 0.07A at 120 °C.

Figure 18 summarizes the temperature increases as a function of applied currents at 80°C, 100°C and 120°C. The temperature rising due to joule heating increases as the applied current increases for the three ambient temperatures.

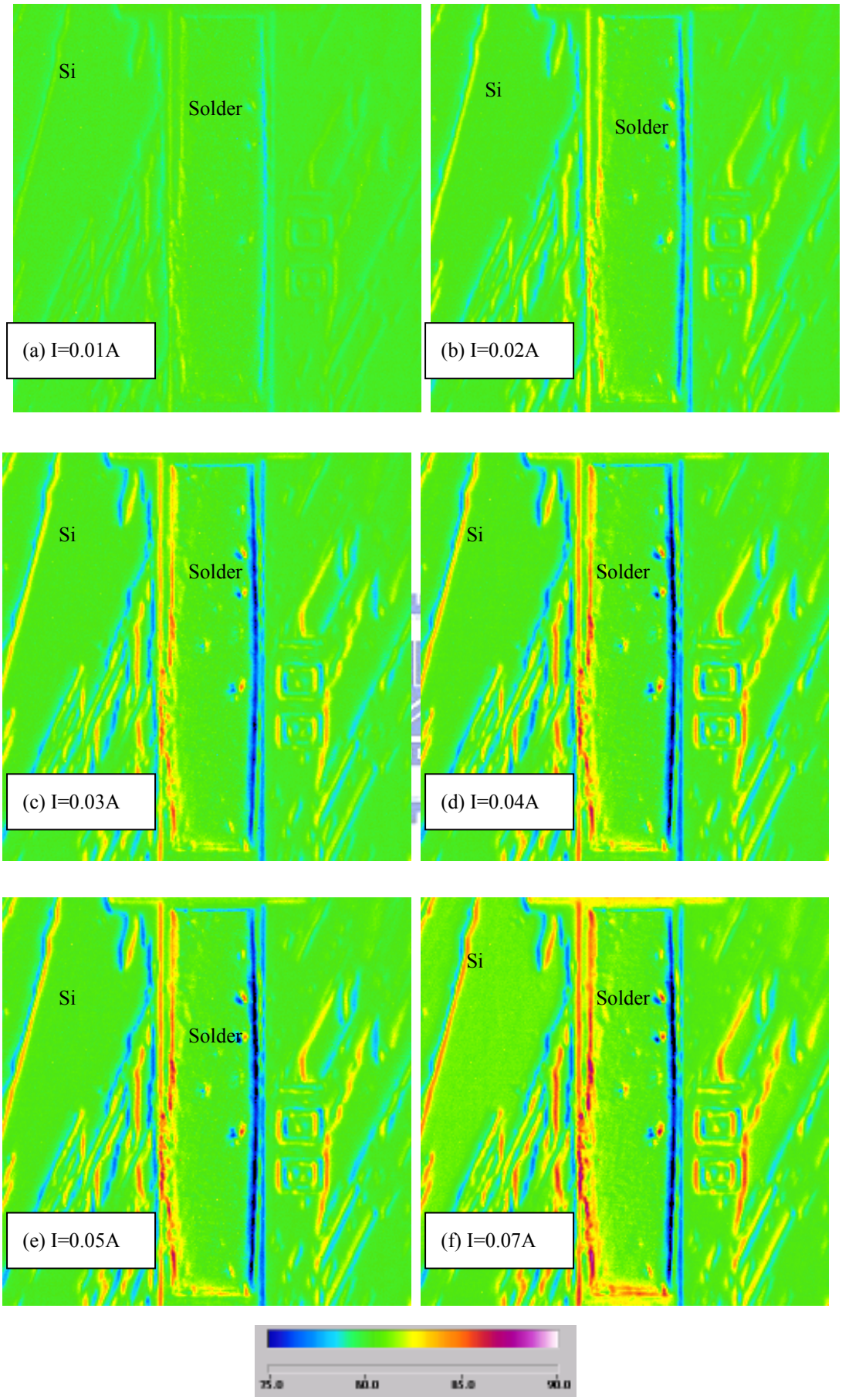
Si
Solder
(a) I=0.01A
Si
Solder
(b) I=0.02A
Si
Solder
(c) I=0.03A
Si
Solder
(d) I=0.04A
Si
Solder
(e) I=0.05A
Si
Solder
(f) I=0.07A

,

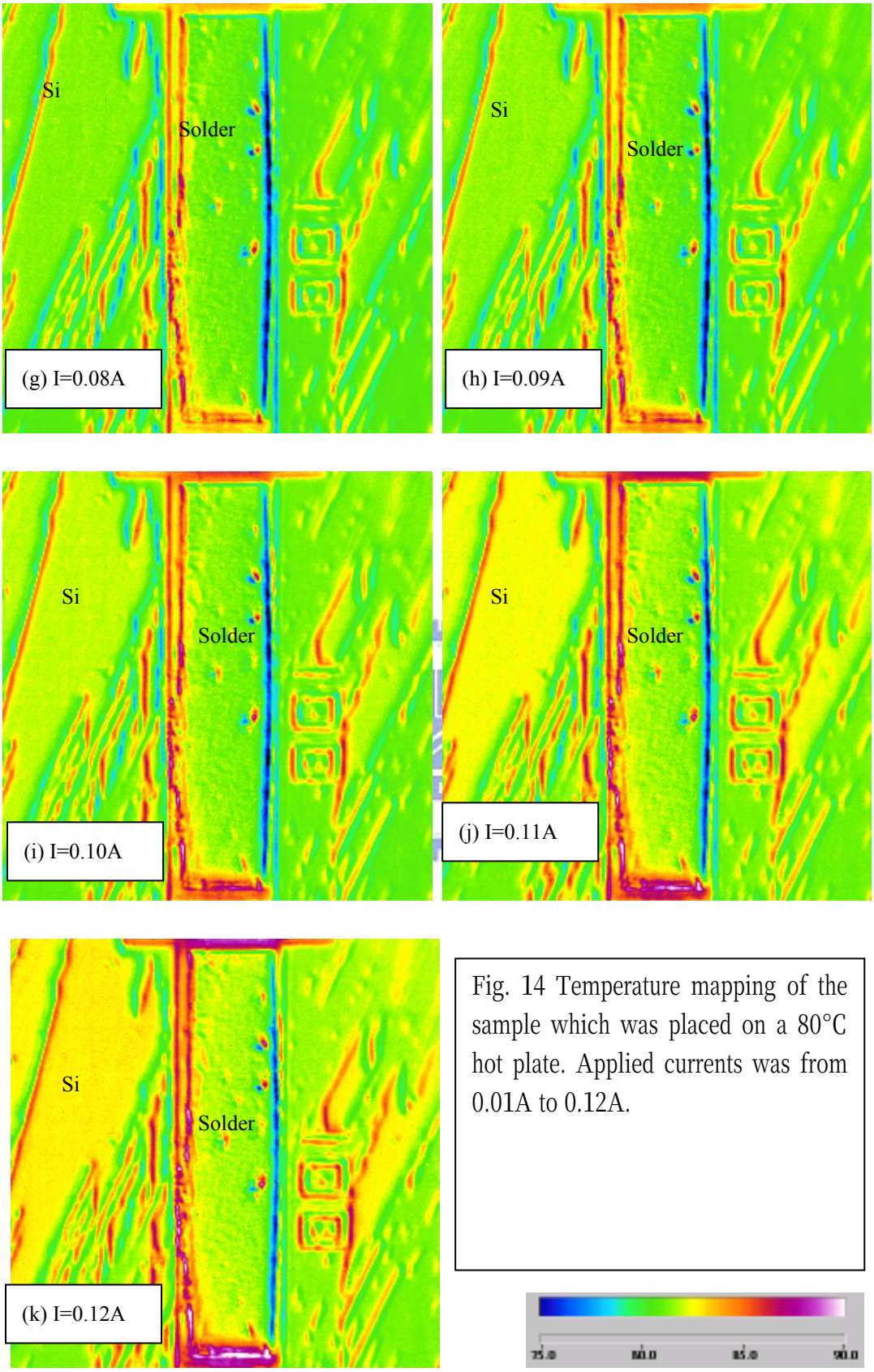

Fig. 14 Temperature mapping of the sample which was placed on a 80°C hot plate. Applied currents was from 0.01A to 0.12A.

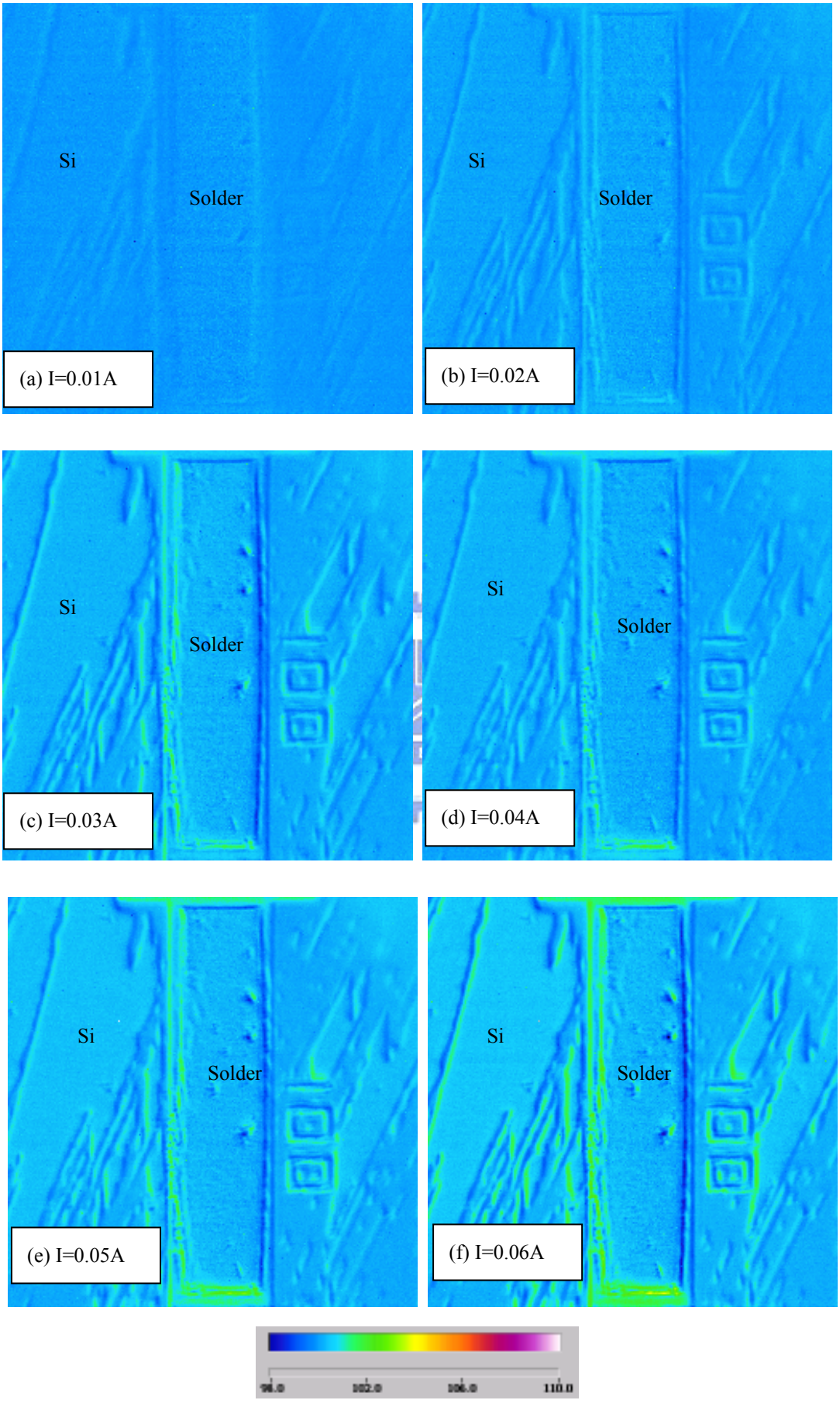
Si
Solder
(a) I=0.01A
Si
Solder
(b) I=0.02A
Si
Solder
(c) I=0.03A
Si
Solder
(d) I=0.04A
Si
Solder
(e) I=0.05A
Si
Solder
(f) I=0.06A
98.0
102.0
106.0
110.0

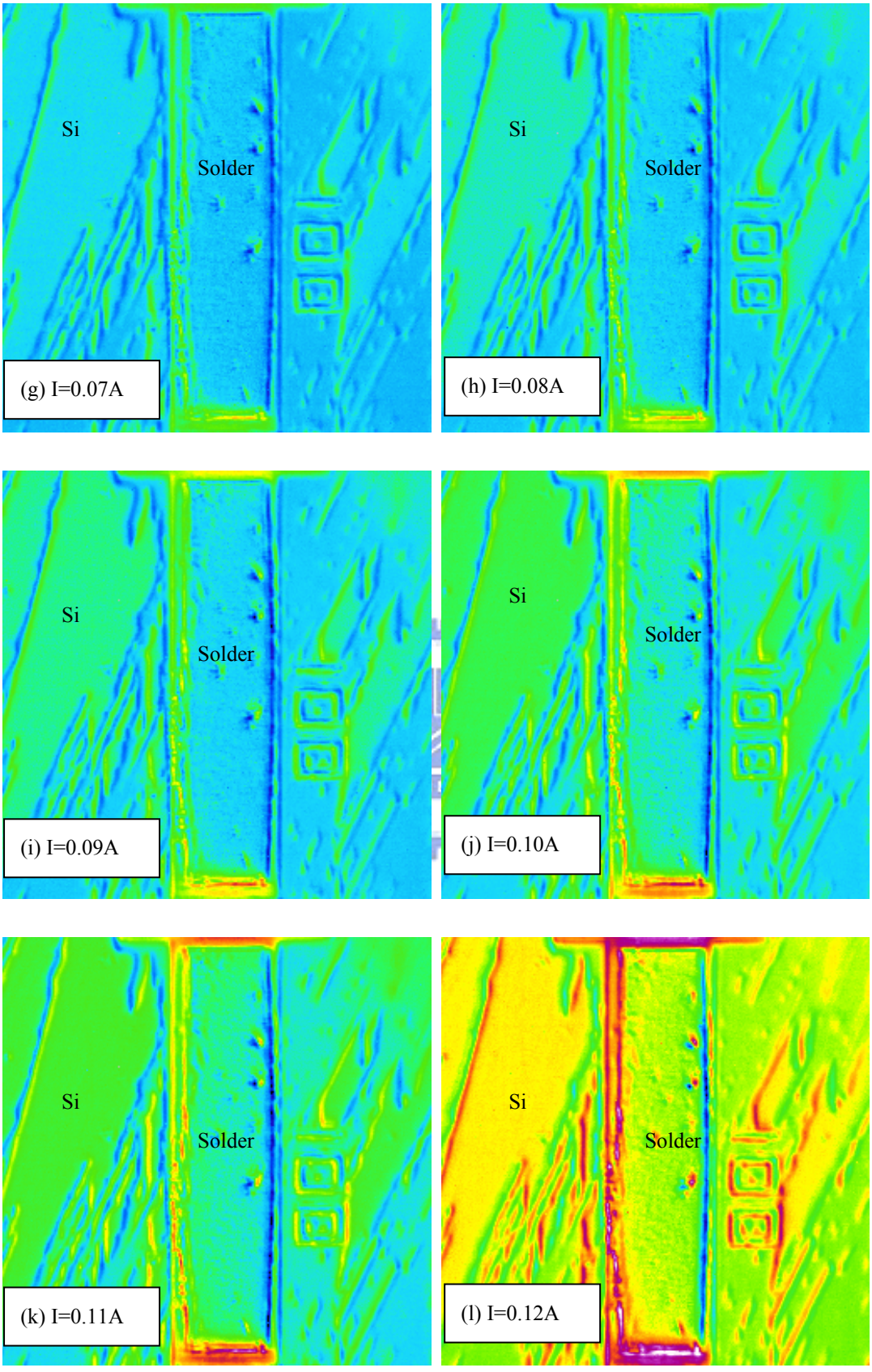

Fig. 15 Temperature mapping of the sample which was placed on a 100°C hot plate. Applied currents was from 0.01A to 0.12A.

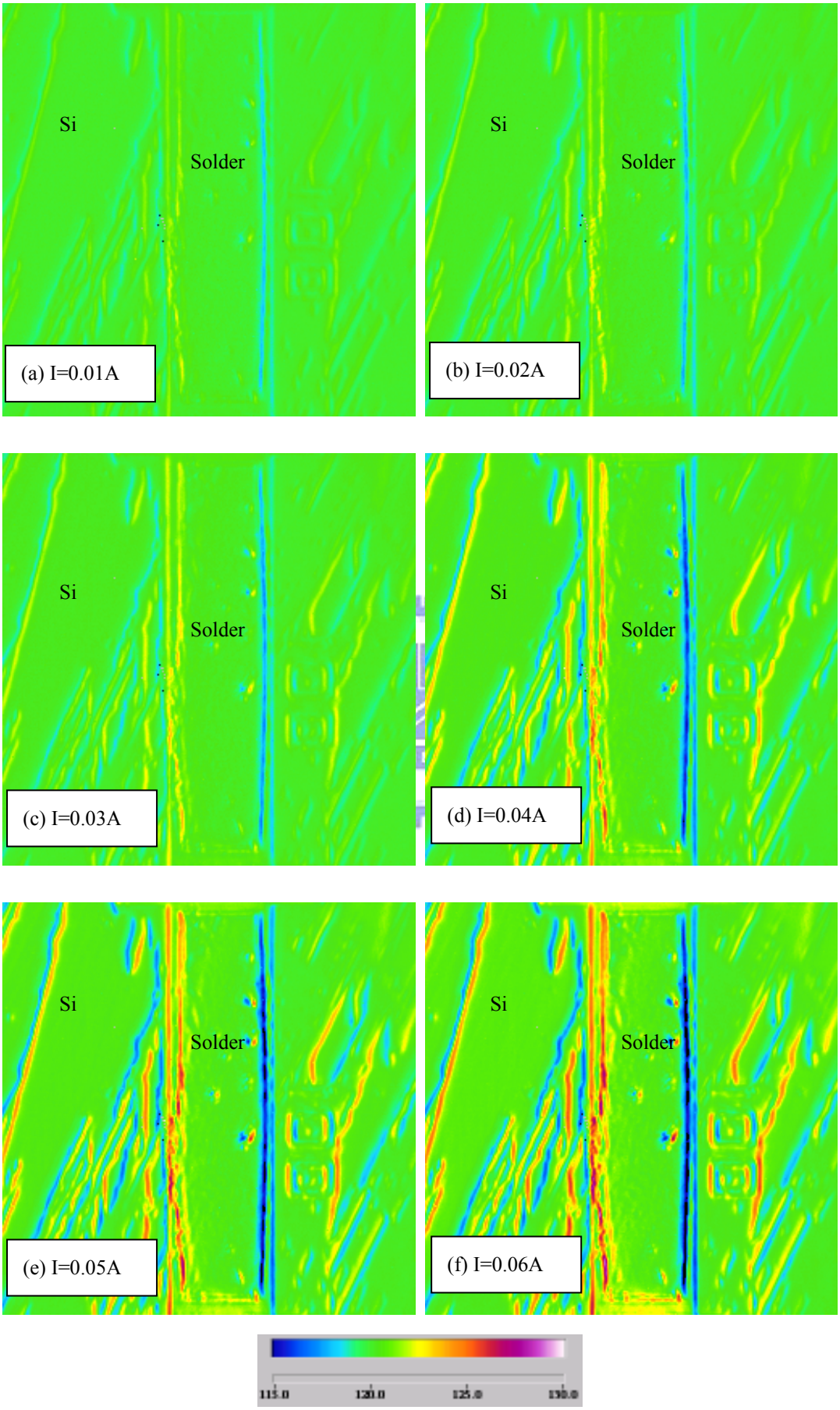
Si
Solder
(a) I=0.01A
Si
Solder
(b) I=0.02A
Si
Solder
(c) I=0.03A
Si
Solder
(d) I=0.04A
Si
Solder
(e) I=0.05A
Si
Solder
(f) I=0.06A
115.0
120.0
125.0
130.0

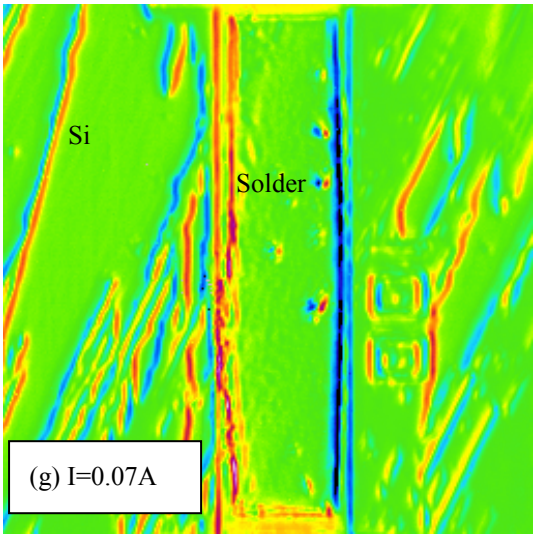

Fig. 16 Temperature mapping of the sample which was placed on a 120°C hot plate. Applied current was from 0.01A to 0.07A.

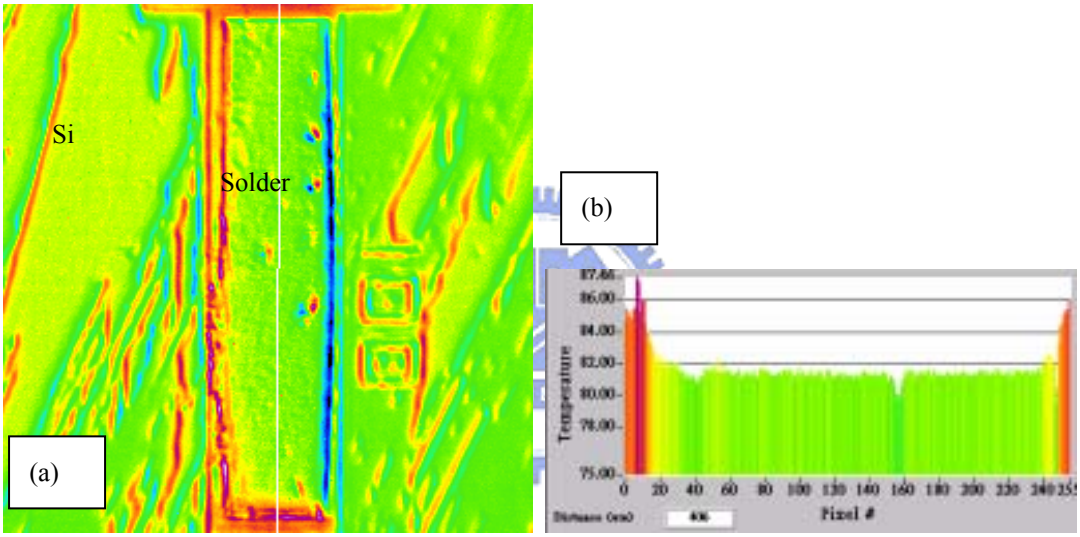

Fig. 17 (a) Temperature Mapping of the sample which was placed on a 80°C hot plate. Applied current was 0.1A. (b)The temperature profile along the white line in (a).

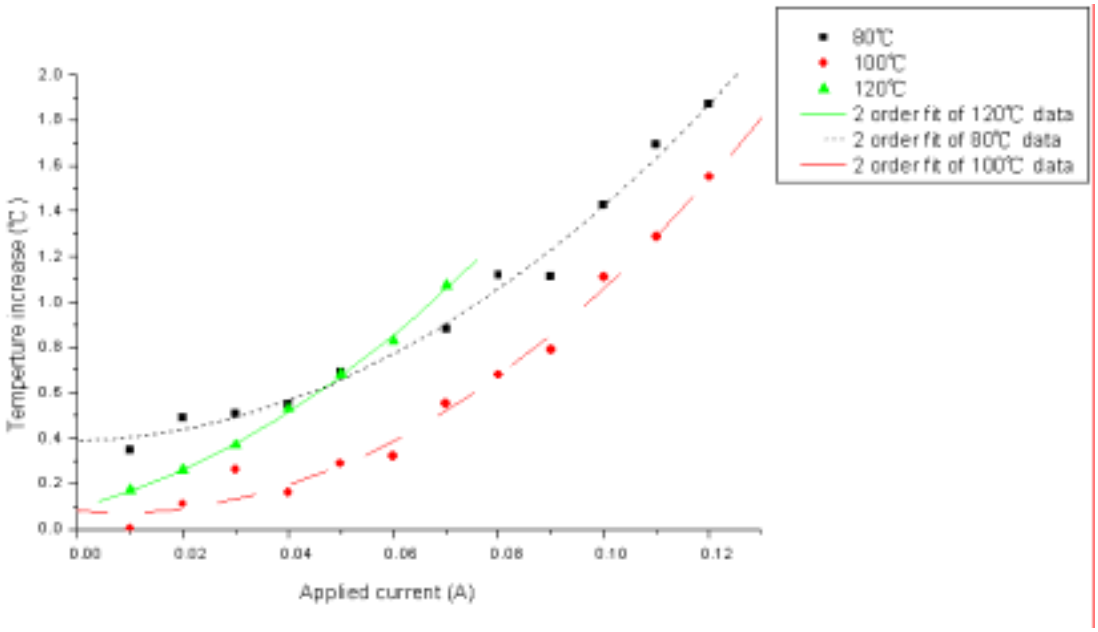

Fig. 18 The temperature increase verses applied current.

3.2 Microstructure Evolution during Electromigration

Figure19 through 26 show the typical microstructure evolution during current stressing for various current density at 80°C, 100°C and 120°C. After the reflow of the solder, Pb-rich region was surrounded by Sn-rich region. During current stressing Pb-rich region grew up due to solid state aging. After current stressing, depletion occurred at the cathode end of the stripe, and extrusions formed at the anode end of the stripe.

Figure 19 (b) shows the SEM images of the cathode end of the solder stripes after the under current stressing of 9.7 x 10^3A/cm^2 at 80°C for 24 hrs Pb-rich region grew up due to solid state aging. With longer current stressing for 72hrs, the sizes of Pb-rich region do not change very much. There was some residual flux on the Ti at right side. Figure 20 (a) show the SEM images of the cathode end of the solder stripes before current stressing of 4.9 x 10^4A/cm^2 at 80°C. At the corners of the edge, the solder did not wetting well during reflow process. After the current stressing of 4.9 x 10^4A/cm^2 at 80°C, it could be observed that IMCs appear near the edge. The deplete region which is defined by the IMCs region. It was found that, at upper and lower corners of the edge, the depletion length was longer than that at center. It was due to polishing process, which made the solder at ther corners much thinner than that at center. Figure 20 (c) shows SEM image of the cathode end of the solder stripe after the current stressing of 4.9 x 10^4A/cm^2 at 80°C for 72hrs. The depletion was much more than that under the stressing for 24hrs. A hillock formed 60 μm away form the edge. Figures 21 (a) and (b) show the SEM images of the cathode end of the solder stripe before and after the current stressing of 8 x 10^4A/cm^2 at 80°C for 72hrs, respectively.The delpletion region observed by SEM was enlarged than that in Fig. 20 (c). There was also a hillock formed at approximately 50 μm away from the edge. Figures 22 (b) and (c) show the SEM images of the cathode end of the solder stripe after the current stressing of 9.1 x 10^3A/cm^2 at 100°C for 72hrs and 144hrs, respectively. The depleted

region was slightly increasing for 144hrs current stressing. Figures 23 (b) shows the SEM image of the cathode end of the solder stripe after the current stressing of 3 x 10^4A/cm^2 at 100°C for 72 hrs. The depleted region was measured to be 17 μm. At upper-right hand side of the depleted region ,some residual Pb-rich region was found among IMCs. Figure 24 (b) shows the SEM image of the cathode end of the solder stripe after the current stressing of 5.4 x 10^4A/cm^2 at 100°C for 72 hrs. The depletion region was measured to be 27 μm. Figure 25 (a) and 25 (b) show the SEM images of the cathode end of the solder stripe before the current stressing of 9.9 x 10^3A/cm^2 at 120°C for 72hrs. Some IMCs were observed before the current stressing, which was due to polish process. After the current stressing of 9.9 x 10^3A/cm^2 at 120°C for 72hrs, the IMCs region slightly increased. Figure 26 (b) shows the SEM image of the cathode end of the solder stripe after the current stressing of 3 x 10^4A/cm^2 at 120°C for 72 hrs. The IMCs appeared after the current stressing. Again, there were some residual Pb-rich regions among the IMCs. It is hard to calculate the depleted volume by SEM images only because it hard to define the depletion region. Therefore, we employed AFM to measure the depletion volume.

Figure 27 shows the cross-sectional SEM image for the solder Blech structure. The morphology of the IMC is scallop-type and the average thickness is 0.87 μm. This scallop-type IMC was analyzed to be Cu_6Sn_5. According to the literature [2], the eutectic SnPb solder joints consist of Cu_6Sn_5 (η -phase) and Cu_3Sn (ε -phase) intermetallic layers at the interface of eutectic SnPb solder and a copper foil. However, only η -phase presents and no ε -phase was formed in this study. The absence of the Cu_3Sn may be due to that the copper layer in the UBM was only 0.4 μm. There is no enough Cu for the formation of the Cu_3Sn IMC.

In conclusion, as shown in Figs. 20(b) (c), Fig. 21 (b) (c), Fig. 23 (b), Fig. 24 (b), Fig. 25 (b) and Fig. 26 (b). The IMC appeared on the cathode end of the solder after current stressing. However, IMCs could not be observed at cathode end after the current stressing

of 9.7 x10^3 at 80°C up to 162hrs, as shown in Figs. 19(a) to 19(d). As shown in Figs. 20(a) to (c), solder depleted form the edge and broadened the depletion region as stressing time increased. Due to lower drift velocity at lower stressing temperature and current density, volume depletion in the cathode end was not serious.

Figures 28 (a) and 28 (b) show the AFM 3D- images of the cathode end before and after the current stressing of 3x10^4A/cm^2 at 100°C for 72hrs, it was clearly seen that the morphology of IMC is scallop type after solder was depleted. By estimating average height of this region, we can obtain the average thickness of IMC to be 0.894 μm.

Figures 29 to 36 show the microstructure evolution at the anode end during current stressing. For most cases, hillocks were observed at the anode end of the solder. However, no obvious hillock formation was found in sample with lower stressing current and temperature, as shown in Fig. 29.

(a) 0 hr (b) 24 hrs

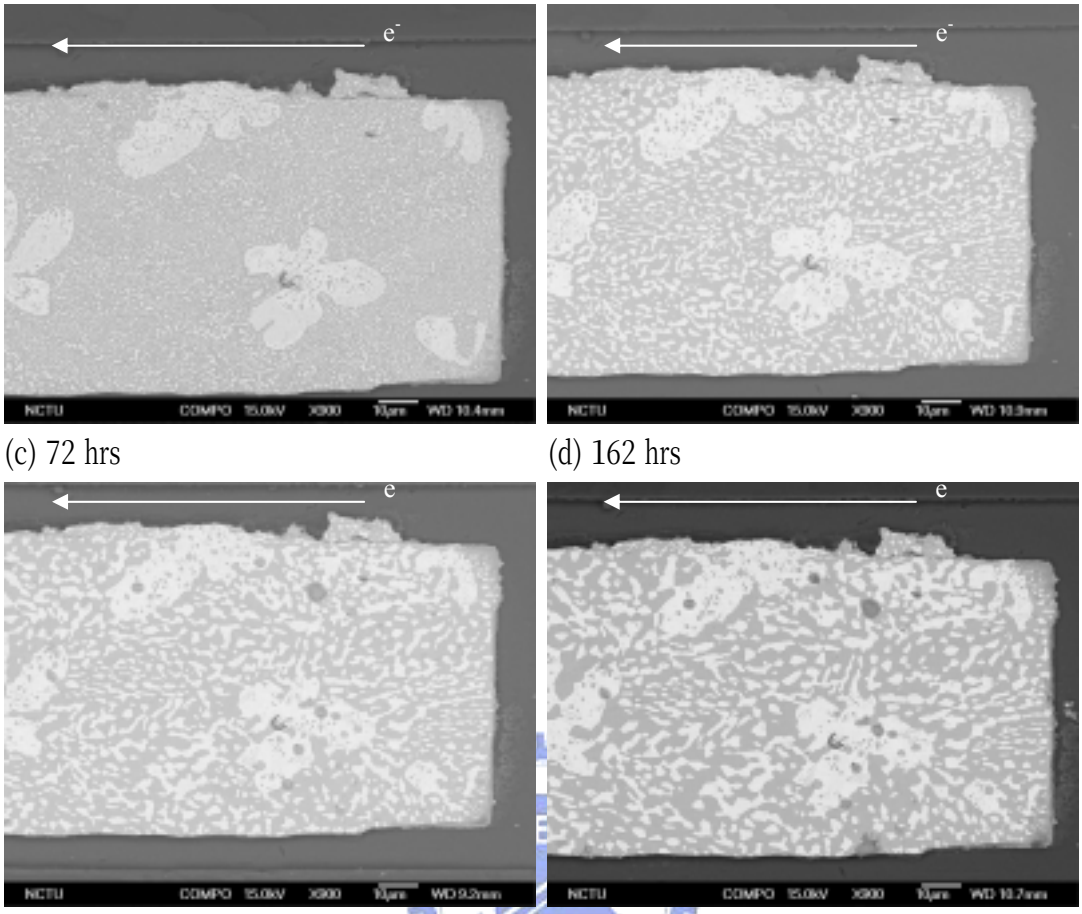

(c) 72 hrs (d) 162 hrs

Fig. 19 SEM images of the cathode end of the solder stripes after the under current stressing of 9.7×10^{3} A/cm^{2} at 80°C for (a) 0 hr (b) 24 hrs(c) 72 hrs (d) 162 hrs

,

(a) 0 hr (b) 24 hrs

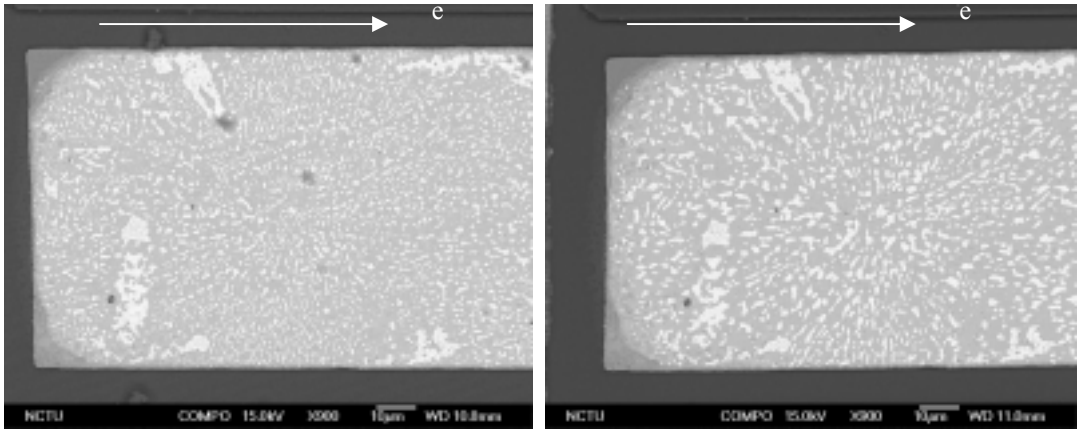

(c) 72 hrs

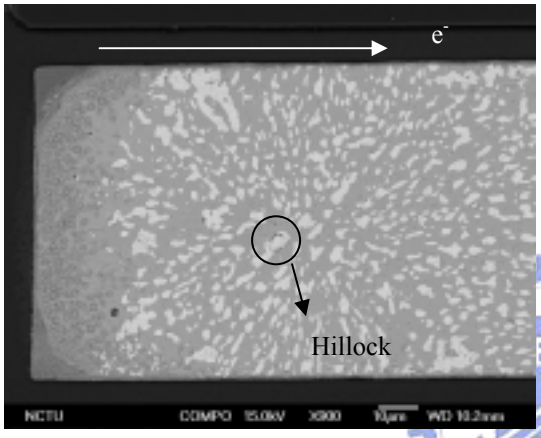

Fig. 20 SEM images of the cathode end of the solder stripes after current stressing of $4.9 \times 10^4 A/cm^2$ at 80°C (a) 0 hr (b) 24hr (c) 72 hrs.

(a) 0 hrs (b) 72 hrs

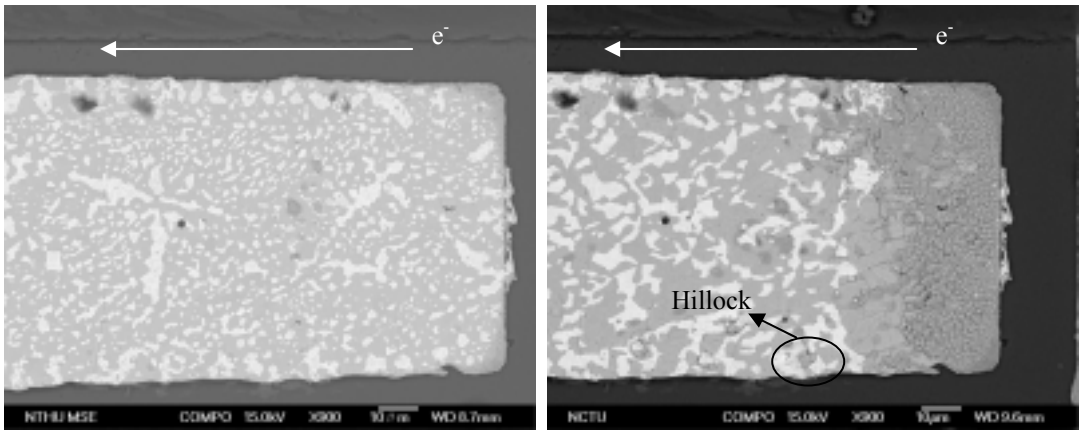

Fig. 21 SEM images of the cathode end of the solder stripes after current stressing of $8 \times 10^4 A/cm^2$ at 80°C. (a) 0 hr (b) 72 hrs.

(a) 0 hr (b) 72 hrs

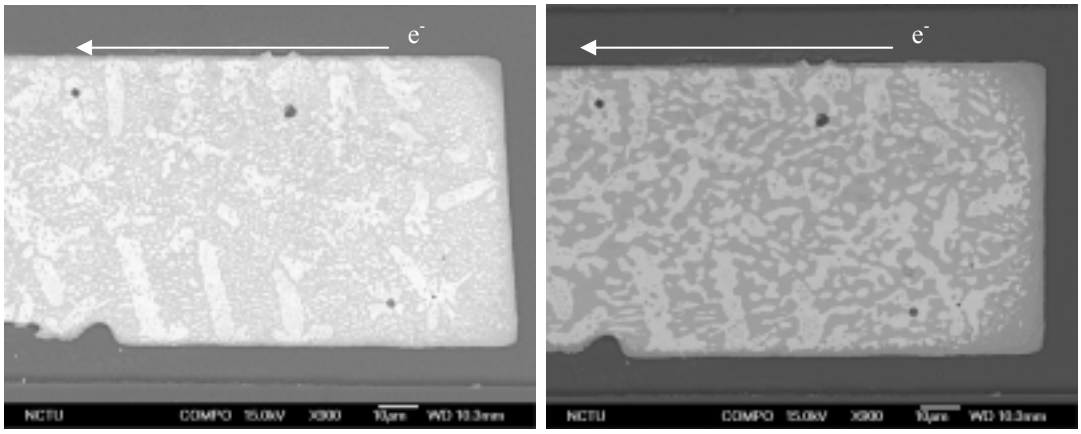

(c) 144 hrs

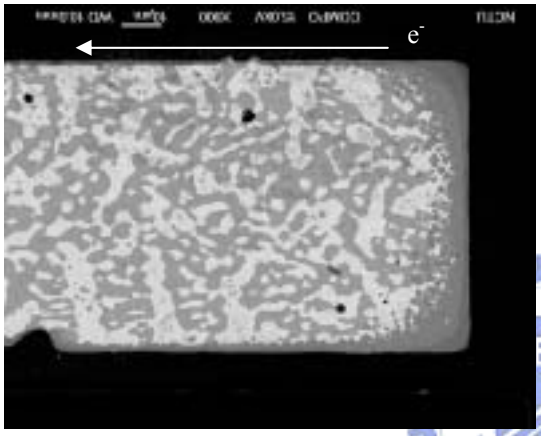

Fig. 22 SEM images of the cathode end of the solder stripes after the current stressing of $9.1 \times 10^{3} A/cm^{2}$ at 100°C for (a) 0 hr (b) 72 hrs (c) 144 hrs

(a) 0 hr (b) 72 hrs

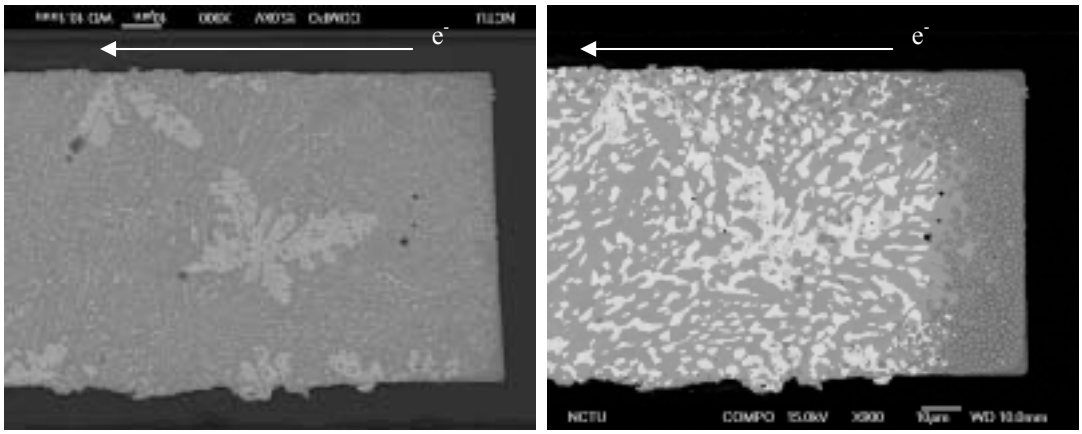

Fig. 23 SEM images of the cathode end of the solder stripes after current stressing of $3 \times 10^{4} A/cm^{2}$ at 100°C. (a) 0 hrs (b) 72 hrs

(a) 0 hr (b) 72 hrs

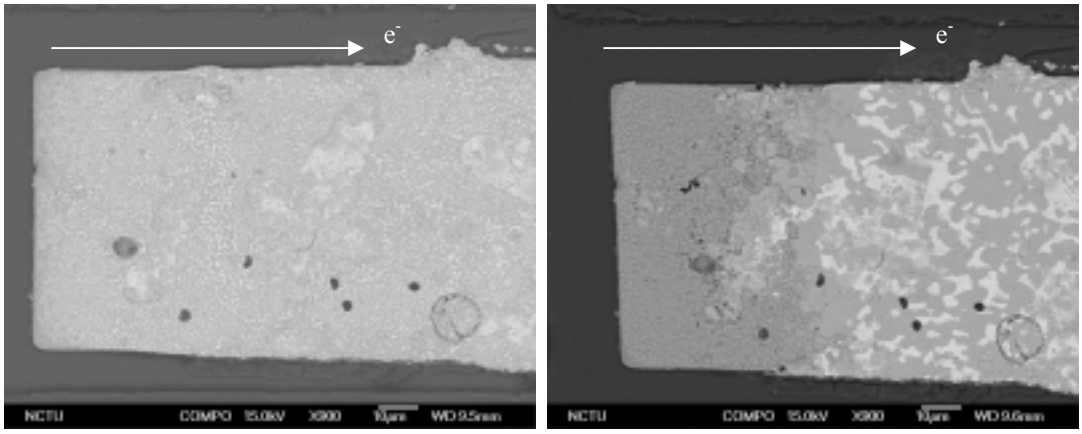

Fig. 24 SEM images of the cathode end of the solder stripes after the current stressing of $5.4 \times 10^{4} A/cm^{2}$ at 100°C for (a) 0 hr (b) 72 hrs

(a) 0 hr (b) 72 hrs

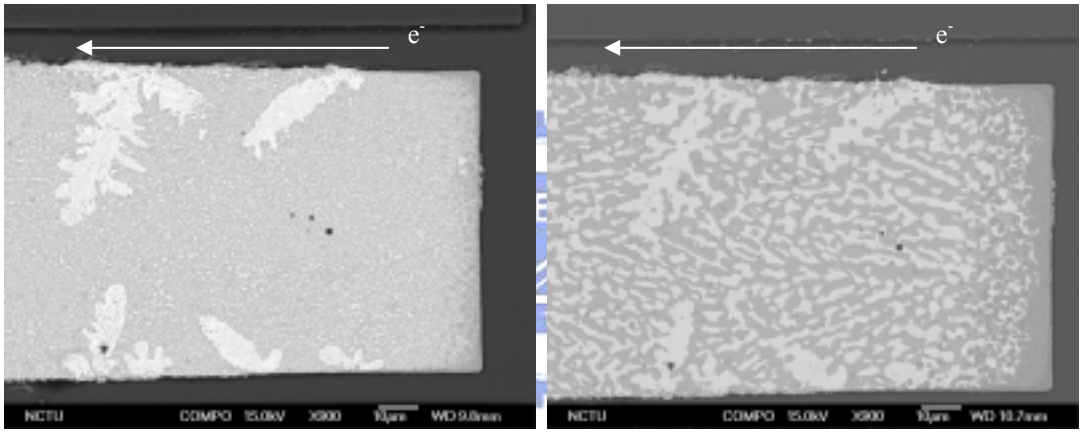

Fig. 25 SEM images of the cathode end of the solder stripes after current stressing of $9.9 \times 10^{3} A/cm^{2}$ at 120°C for (a) 0 hr (b) 72 hrs

(a) 0 hr (b)72 hrs

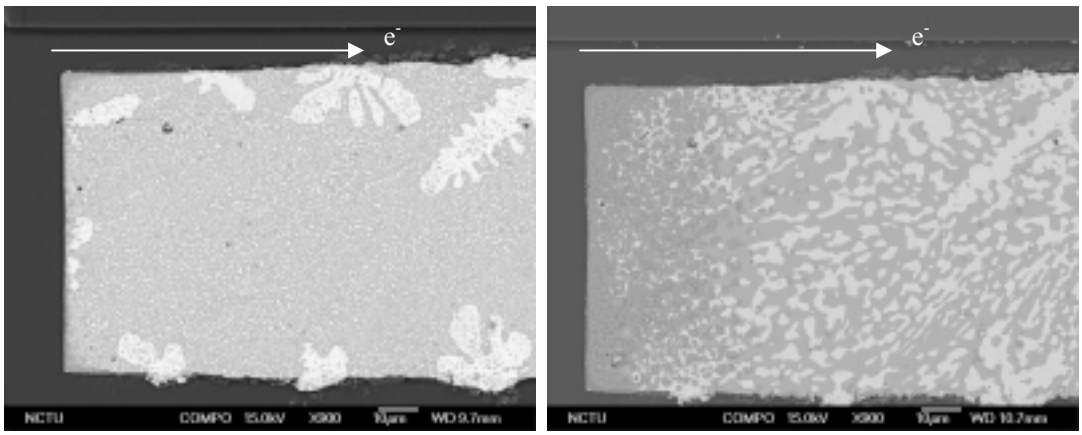

Fig. 26 SEM images of the cathode end of the solder stripes after current stressing of $3 \times 10^{4} A/cm^{2}$ at 120°C for (a) 0 hr (b) 72 hrs

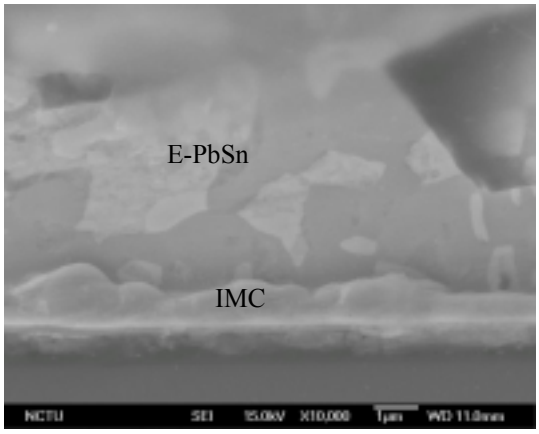

Fig. 27 Cross-sectional SEM image of the solder stripe after the reflow at 210°C for 4s

(a) 0 hr (b) 72 hrs

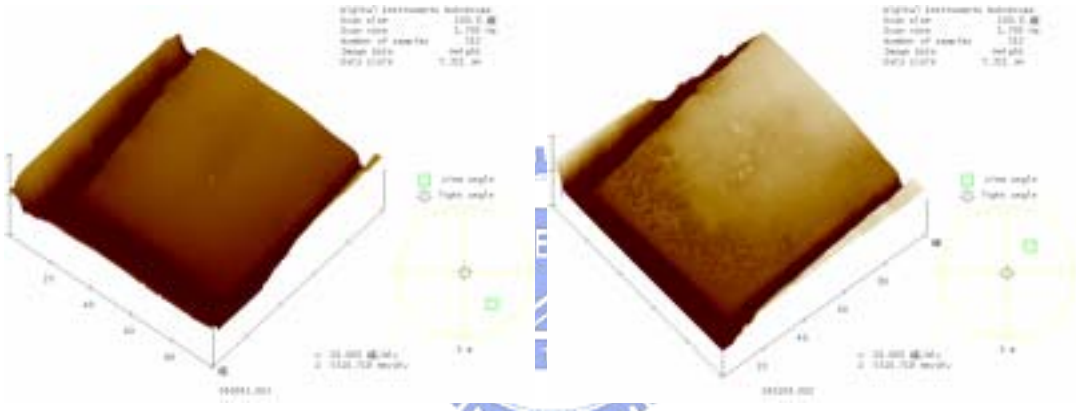

Fig. 28 3-D AFM images of the cathode end of the solder stripes after the sample after under current stressing of $3 \times 10^{4} A/cm^{2}$ at 100°C. (a) before current stressing (b) After 72 hr s current stressing.

(a) 0 hr (b) 24 hrs

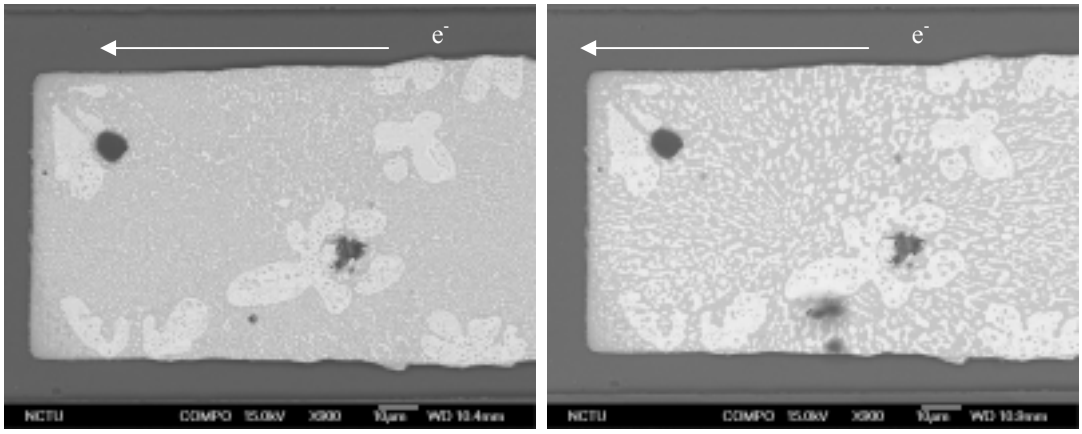

(c) 72hrs (d) 162 hrs

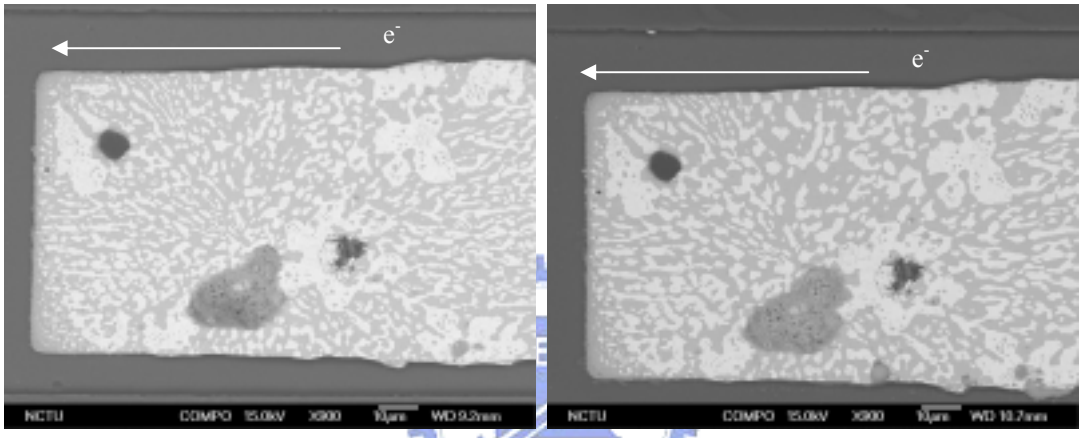

Fig. 29 SEM images of the anode end of the solder stripes after current stressing of 9.7 X 10^3 A/cm^2 at 80°C for (a) 0 hr (b) 24 hrs(c) 72 hrs (d) 162 hrs

(a) 0 hr (b) 24 hrs

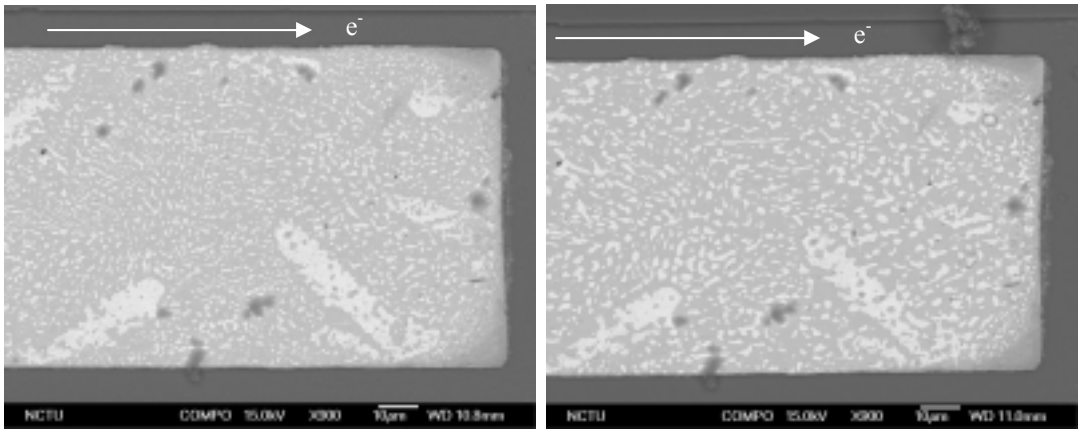

(c) 72 hrs

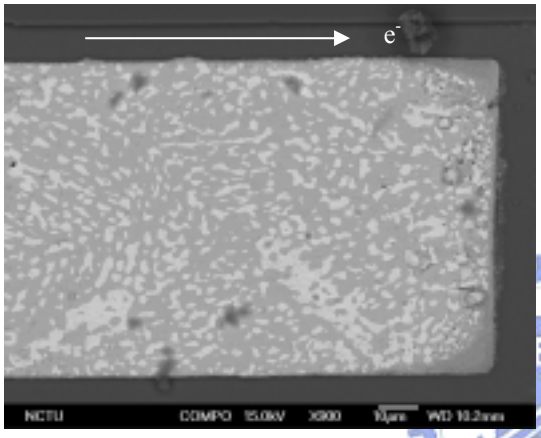

Fig. 30 SEM images of the anode end of the solder stripes after current stressing of 4.9 X 10^4A/cm^2 at 80°C for (a) 0 hr (b) 24 hrs (c) 72hrs

(a) 0 hr (b)72 hrs

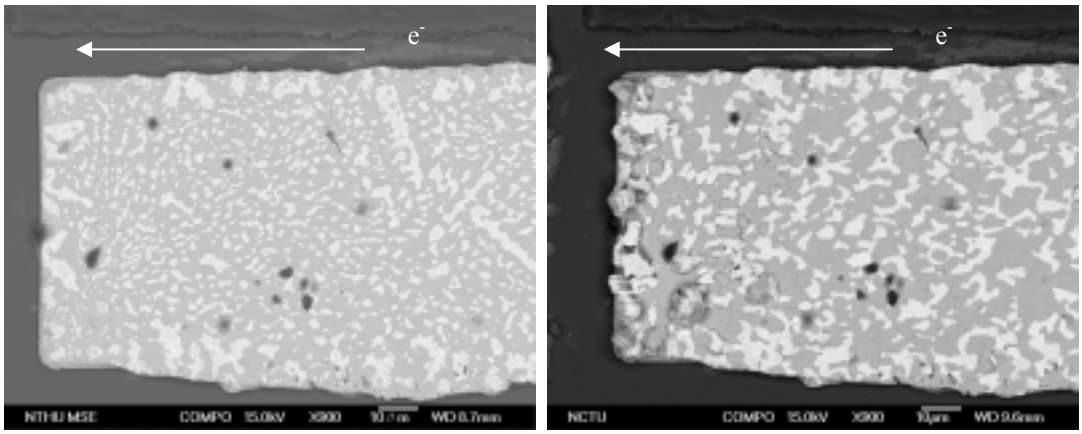

Fig. 31 SEM images of the anode end of the solder stripes after current stressing of 8 X 10^4A/cm^2 at 80°C for (a) 0 hr (b) 72 hrs

(a) 0 hr (b) 72 hrs

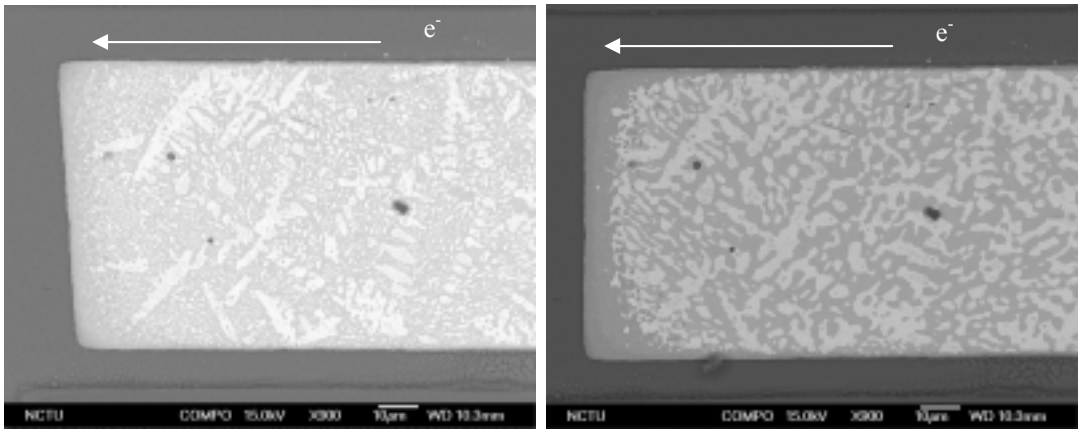

(c) 144 hrs

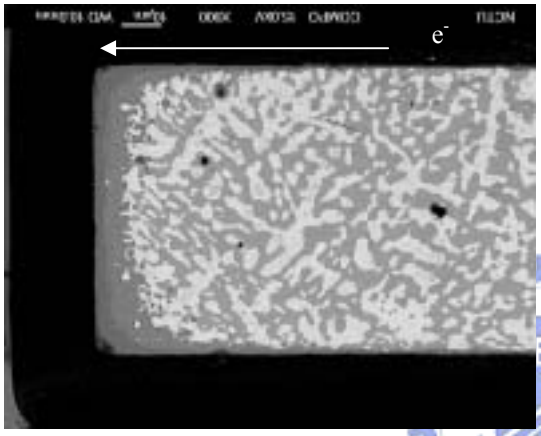

Fig. 32 SEM images of the anode end of the solder stripes after current stressing of 9.1 X 10^3A/cm^2 at 100°C for (a) 0 hr (b) 72 hrs (c) 144 hrs

(a) 0 hr (b)72 hrs

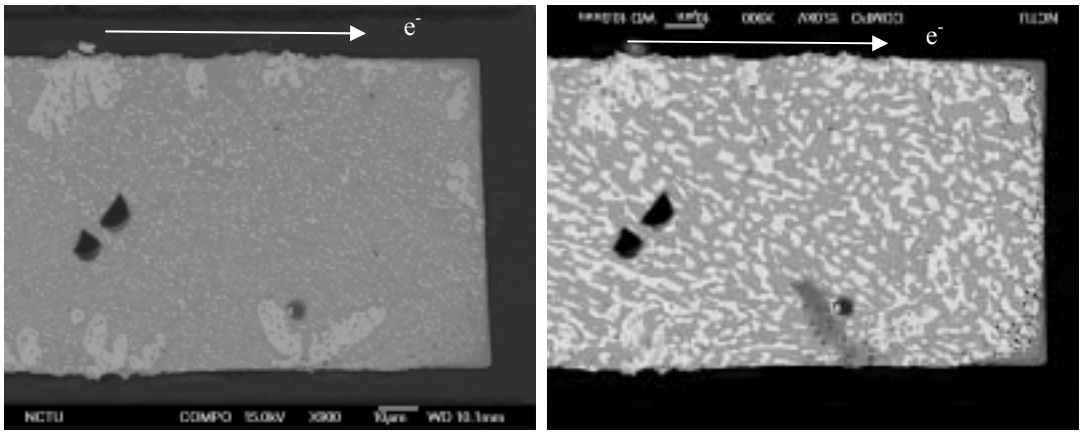

Fig. 33 SEM images of s the anode end of the solder stripes after current stressing of 3 X 10^4A/cm^2 at 100°C for (a) 0 hr (b) 72 hrs

(a) 0 hr (b) 72 hrs

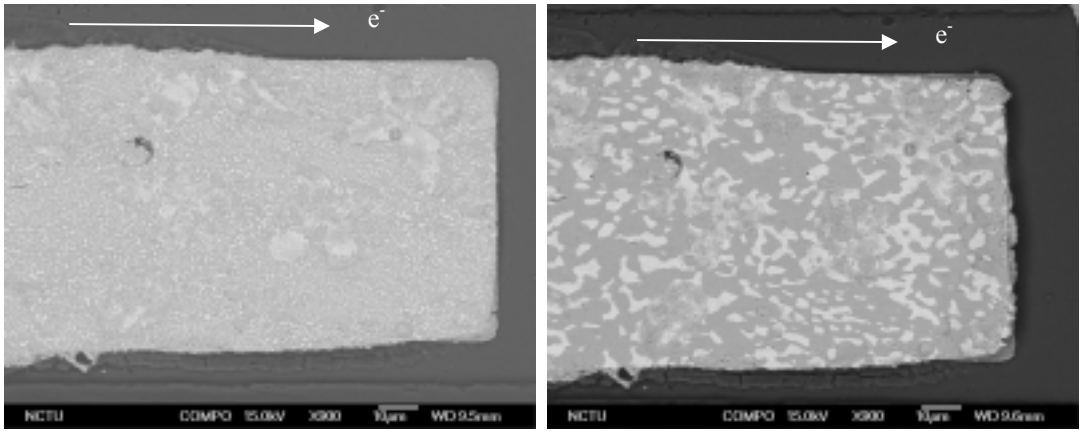

Fig. 34 SEM images of the anode end of the solder stripes after current stressing of $5.4 \times 10^{4} A/cm^{2}$ at 100°C for (a) 0 hr (b) 72 hrs

(a) 0 hr (b) 72 hrs

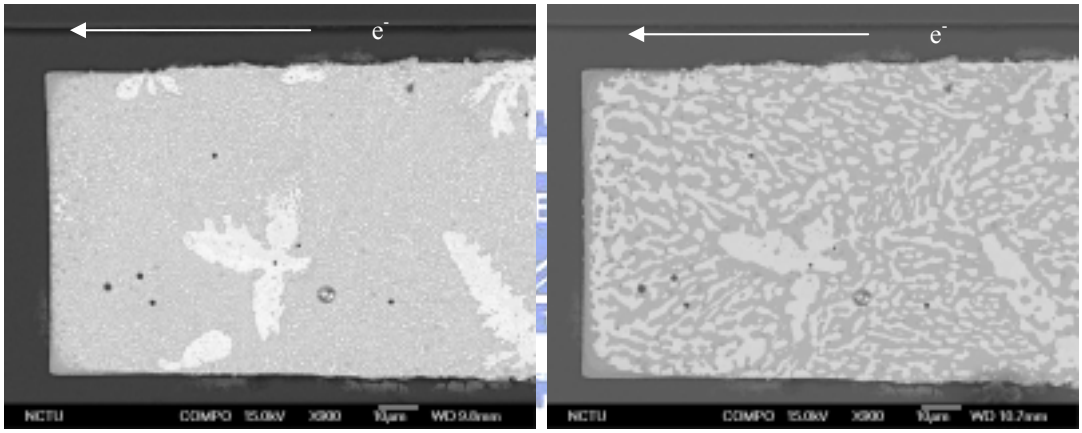

Fig. 35 SEM images of the anode end of the solder stripes after current stressing of $9.9 \times 10^{3} A/cm^{2}$ at 120°C for (a) 0 hr (b) 72 hrs

(a) 0 hr (b) 72 hrs

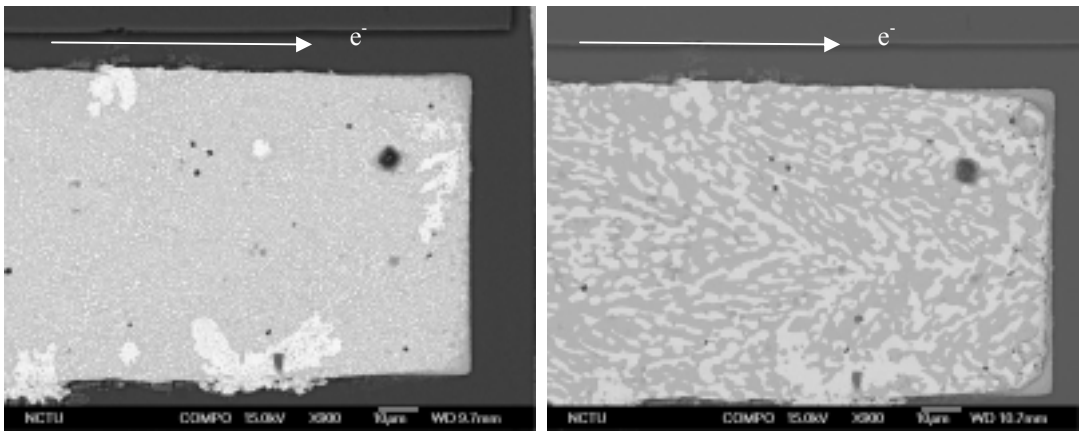

Fig. 36 SEM images of the anode end of the solder stripes after current stressing of $3 \times 10^{4} A/cm^{2}$ at 120°C for (a) 0 hr (b) 72 hrs

3.3 Measurement of Electromigration Parameters

Upon current stressing, depletion of solder occurred on the cathode end and extrusion formed on the anode end of the solder strip, as seen in Figs. 37(a) and 37(b). Figure 37(a) shows the plan-view SEM image in the cathode end of a SnPb solder strip before current stressing, and it also shows the thickness profile along the line in the SEM image. After the current stressing of 3×10^4 A/cm^2 at 120 °C for 72 hours, its microstructure is shown in Fig. 37(b), and the corresponding thickness profile is shown in the figure too. The two thickness profiles were plotted together, showing the depletion in the cathode end, as shown in Fig. 37(c). Depletion of solder occurred on the cathode end due to electromigration, causing the IMCs to be visible from top view observation, as observed in the AFM image in Fig. 37(b).

To measure the depletion volume for calculation drifting velocity, AFM scanning was performed to obtain three-dimensional surface profiles before and after the current stressing, as seen in Fig. 28(a) and 28(b) respectively. By estimating the volume difference between the two profiles, depletion volume and thus drift velocity can be calculated. The depletion volume for each sample is tabulated in Table 3. Appropriate scanning area was chosen for each sample. Table 4 shows the calculated drift velocity for each sample. It increases with the increase of stressing current for the same temperature.

Figure 39 shows the measured drift velocity as a function of applied current density at 80, 100, and 120 °C. The drift velocity increases when the applied current increases. By extrapolating to the zero drift velocity, the calculated threshold current density is -1.2×10^3 A/cm^2 at 80 °C, -1.8×10^3 A/cm^2 at 100 °C, and 2.9×10^3 A/cm^2 at 120 °C, respectively. The negative values are incorrect since the threshold current density should be a positive value. It may be due to the current crowding effect occurring on both cathode and anode ends in Blech specimens.

Tu *et al* reported that the current density in the both ends may be one order higher than the average current density in the center of the strip [24]. Therefore, rather than the average current density, it is mainly the current density near the cathode end that migrates the solder away. The activation energy can be obtained from the slope of the plot of ln(V*T/j) against 1/T, as shown in Fig. 39. The measured activation energy was 0.34 eV, which is lower than 0.5 eV calculated from MTTF measurement [15] and 0.77 eV by resistometric measurement [13]. With the activation energy, the values of D_0Z^* could be calculated. The values are shown in Table 5, and the average value was -9.71×10^6 cm^2/sec.

(a) Under current stressing of 9.7 x 10^3 A/cm^2 at 80°C

Area	69.37 μm x 68.36 μm	69.37 μm x 58.59 μm	69.34 μm x 39.06 μm
Depletion volume after 72 hr	551.77 μm^3	467.44 μm^3	385.41 μm^3
Depletion volume after 162 hr	775.58 μm^3	639.09 μm^3	504.29 μm^3

(b) Under current stressing of 4.9 x 10^4 A/cm^2 at 80°C

Area	75.88 μm x 48.93 μm	75.88 μm x 39.06 μm	75.88 μm x 31.84 μm
Depletion volume after 72 hr	784.62 μm^3	658.05 μm^3	696.93 μm^3

(c) Under current stressing of 8 x 10^4 A/cm^2 at 80°C

Area	70.12 μm x 68.36 μm	70.12 μm x 58.59 μm	70.12 μm x 39.06 μm
Depletion volume after 72 hr	1750.58 μm^3	1700.11 μm^3	1528.31 μm^3

(d) Under stressing of 9.1 x 10^3 A/cm^2 at 100°C

Area	72.07 x 68.36 μm	72.07 x 58.59 μm	72.07 μmx39.06 μm
Depletion volume after stressing 72hr	849.09 μm3	813 μm^3	771.34 μm^3
Depletion volume after 144 hr	997.87 μm^3	996.68 μm^3	778.85 μm^3

(e) Under current stressing of 3 x 10^4 A/cm^2 at 100°C

Area	77.73 μm x 68.36 μm	77.73 μm x 58.59 μm	77.73 μm x 39.06 μm
Depletion volume after 72 hr	1099.25 μm^3	954.17 μm^3	822.34 μm^3

(f) Under current stressing of 5.4 x 10^4 A/cm^2 at 100°C

Area	72.46 μm x 68.36 μm	72.46 μm x 58.59 μm	72.46 μm x 39.06 μm
Depletion volume after 72 hr	2450.24 μm^3	2227.72 μm^3	1352.91 μm^3

(g) Under current stressing of 9.9 x 10^3 A/cm^2 at 120°C

Area	74.41 μm x 68.36 μm	74.41 μm x 58.59 μm	74.41 μm x 39.06 μm
Depletion volume after 72 hr	486.56 μm^3	418.16 μm^3	281.63 μm^3

(h) Under current stressing of 3 x 10^4 A/cm^2 at 120°C

Area	74.61 μm x 68.36 μm	74.61 μm x 58.59 μm	74.61 μm x 39.06 μm
Depletion volume after 72 hr	1793.83 μm^3	1669.52 μm^3	1285.48 μm^3

Table 3 Measurement of depletion volume for each sample by AFM images.

(a) (b)

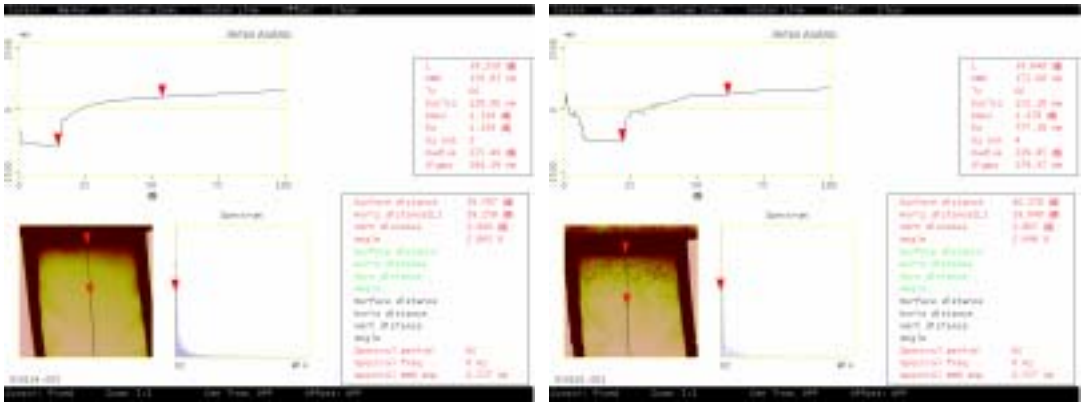

(c)

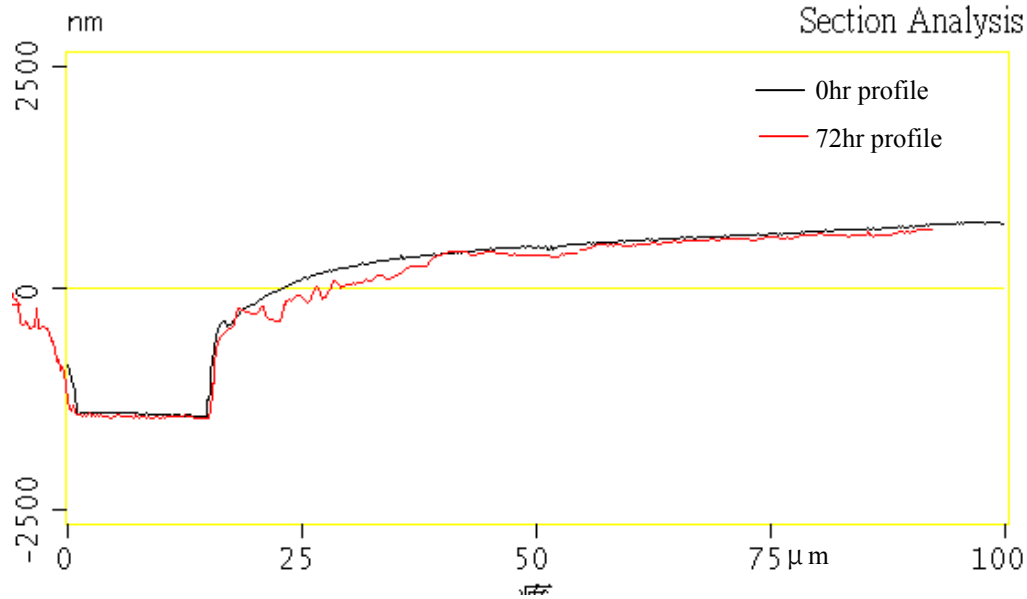

Fig. 37 Thickness profile of the cathode end of the solder stripes (a) before current stressing (b) after current stressing of 3 x 10^4A/cm^2 at 120°C for 72hrs. (c) Comparison of thickness profiles before and after the current stressing.

Stressing condition	Drift velocity(A/sec)	Thickness sample(include IMC)(μ m)	Depletion volume(μm^3)
$9.7x10^3 A/cm^2$ at 80°C 72 hrs	0.112	2.77	551.77
$9.7x10^3 A/cm^2$ at 80°C 162 hrs	0.069	2.77	775.58
$4.9x10^4 A/cm^2$ at 80°C 72 hrs	0.288	1.38	784.62
$8x10^4 A/cm^2$ at 80°C 72 hrs	0.488	1.91	1750.58
$9.1x10^3 A/cm^2$ at 100°C 72 hrs	0.217	2.07	849.09
$9.1x10^3 A/cm^2$ at 100°C 144 hrs	0.131	2.07	997.87
$3x10^4 A/cm^2$ at 100°C 72 hrs	0.346	1.58	1099.25
$5.4x10^4 A/cm^2$ at 100°C 72 hrs	0.641	2.04	2450.24
$9.9x10^3 A/cm^2$ at 120°C 72 hrs	0.152	1.66	486.56
$3x10^4 A/cm^2$ at 120°C 72 hrs	0.603	1.54	1793.83

Table 4 Calculated drift velocity for each sample.

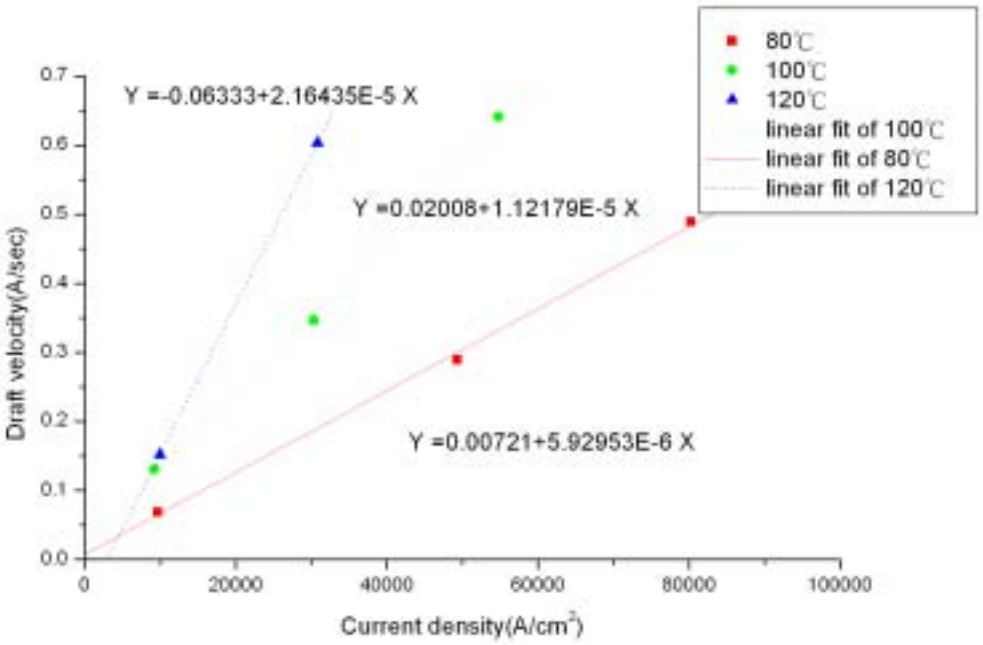

Fig. 38 Plots of drift velocity against current density

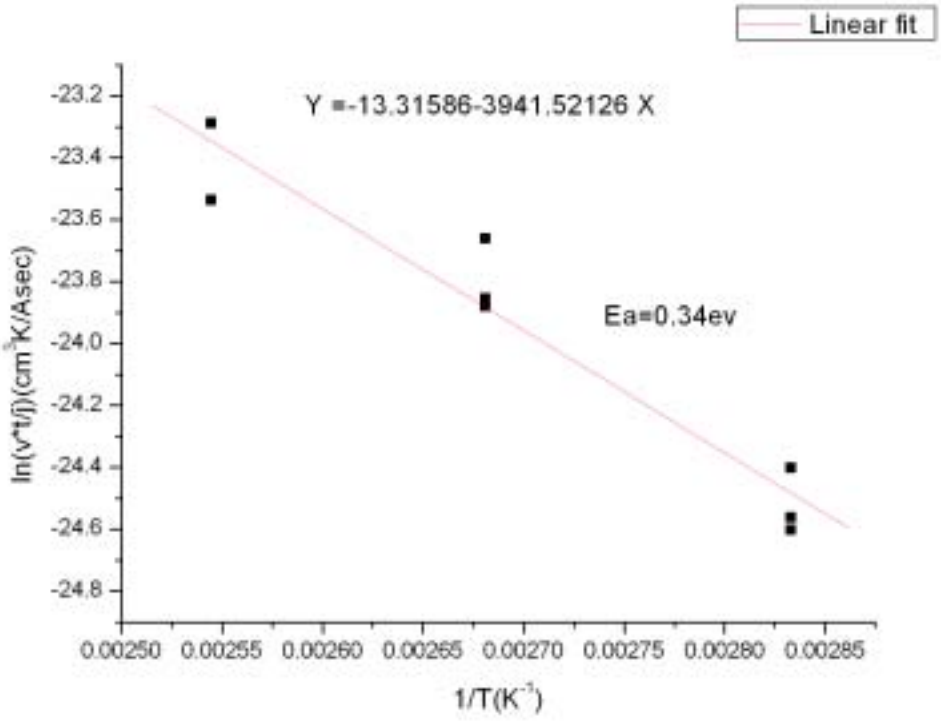

Fig. 39 Plots of ln(v*T/j) against 1/T

Temperature	Current density	$D_0Z^*(cm^2/sec)$
80	9.65E+03	-1.05628E-05
80	4.93E+04	-8.52693E-06
80	8.02E+04	-8.68701E-06
100	9.19E+03	-1.19364E-05
100	3.03E+04	-9.81724E-06
100	5.48E+04	-9.92922E-06
120	9.93E+03	-8.06009E-06
120	3.08E+04	-1.01966E-05
Average		-9.71E-06

Table 5 Evaluate D_0Z^* for each sample.

Chapter 4 Conclusions

We have successfully developed a technique that can measure precisely on the important parameters of solder electromigration. Solder Blech specimens were fabricated on patterned Cu/Ti films in Si trenches. Electromigration eutectic PbSn Blech structure has been investigated. Depletion occurred at the cathode end of the Blech sample, and hillocks were observed at the anode end for most stressing conditions. By employing atomic force microscope to measure the depletion volume on the cathode end, the electromigration rate can be measured. Drift velocity was measured at the current density ranging from 9.1 x 10^3 to 9.7 x 10^4 A/cm^2 at 80, 100, and 120 °C. The drift velocity increased when the applied current increased. The calculated threshold current density is -1.2×10^3 A/cm^2 at 80 °C, -1.8×10^3 A/cm^2 at 100 °C, and 2.9×10^3 A/cm^2 at 120 °C, respectively. The measured activation energy was 0.34 eV. With the activation energy, the values of D_0Z^* was calculated to be -9.71×10^6 cm^2/sec.

References

[1]International Technology Roadmap for Semiconductors, Semiconductor Industry Association, San Jose (2001). See Website http://public.itrs.net/.

[2] K.N. Tu, K Zeng, " Tin-lead (SnPb) solder reaction in flip chip technology, " Materials Science and Engineering R Reports, Vol 34, Issue1, 1(2001).

[3] K.N. Tu, A. M. Gusak, M. Li , " Physics and Materials Challenges for Lead-free Solders "

[4] H. B. Huntington and A.R. Grone, " Current-Induced Masker Motion in Gold Wires, " *J. Phy. & Chem. Solids,* 20, 76 (1961)

[5] I.A. Blech and K.L. Tai, " Measurements of stress gradients generated by electromigration. " Appl. Phys. Lett, 30 387(1977).

[6] P.S. Ho and T. Kwok, " electromigration in metals " Rep. Prog. Phys. 52,301(1989)

[7] K.N. Tu, J.W. Mayer, L.C. Feldman, Macmillan, "Electronic Thin Film Science for Electrical Engineers and Material Scientists," 1992

[8] I.A. Blech and E. Kinsbron, " Electromigration in Thin Gold Films on Molybdenum Surfaces, " Thin Solid Films, Vol. 25,327(1975).

[9] I.A Blech " Electromigration in Thin Aluminum Films on Titanium Nitride, " J. Appl. Phys., Vol. 47, No.4,1203(1976).

[10] A.P. Schwarzenberger, C.A. Ross, J.E. Evetts, and A.L. Greer, " Electromigration in the presence of a Temperature Gradient: Experimental Study and Modeling, " J. Electron. Mater., Vol. 17, No. 5,473(1988).

[11] A. Christou, " Electromigration & Electronic Device Degradation " (1994)

[12] P.F. Tang, A.G. Milnes, C.L. Bauer, and S. Mahajan, " Electromigration in thin films of Au on GaAs. " proc. Mater. Res. Soc., 167,341(1989)

[13] J.Y. Choi, S.S. Lee and Y.C. Joo, " Electromigration Behavior of Eutectic SnPb Solder. " Jpn. J. Appl. Phys. 41, 7487 (2002)

[14] J.R. Black, Proc. Of IEEE, 57, 1587 (1969)

[15] M. Shatzkes and J. R. Lloyd, " A model for conductor failure considering diffusion concurrently with electromigration resulting in a current exponent of 2 " J. Appl. Phys. 59, 3890(1986)

[16] W. J. Choi, E. C. C. Yeh, and K. N. Tu " Mean-time-to-failure study of flip chip

solder joints on Cu/Ni(V)/Al thin-film under-bump-metallization " J. Appl. Phys.94, 5665(2003)
[17] I. A. Blech, J. Appl. Phys. 47, 1203 (1976).
[18] S. Brandenburg and S. Yeh, Proceedings of Surface Mount International Conference and Exhibition, SM198, San Jose, CA, Aug. 23-27, 1998(Edina, MN: SMTA, 1998), p. 337.
[19] C. Y. Liu, Chih Chen, C. N. Liao, and K. N. Tu, Appl. Phys. Lett., **75**, 58 (1999)
[20] C.Y. Liu, Chih Chen, and K.N. Tu, J. Appl. Phys., 88, 5703 (2000).
[21] Q. T. Huynh, C. Y. Liu, Chih Chen, and K. N. Tu, J. Appl. Phys., 89, 4332 (2001).
[22] J. D. Wu, P. J. Zheng, Kelly Lee, C. T. Chiu, and J.J. Lee, 2002 Electronic Components and Technology Conference, p. 452.
[23] J. W. Nah, K. W. Paik, J. O. Suh, and K. N. Tu ,J. Appl. Phys. 94, 7560 (2003).
[24] Everett C. C. Yeh and K. N. Tu, J. Appl. Phys. 88, 5680 (2000).